NOVA SCHOOL OF SCIENCE & TECHNOLOGY

DEPARTMENT OF LIFE SCIENCES

ANA RITA GOMES SOARES

BSc in Biology

DECELLULARIZED FETAL SKELETAL MUSCLE AS AN *IN VITRO* SYSTEM TO STUDY A CONGENITAL MUSCULAR DYSTROPHY

MASTER IN MOLECULAR GENETICS AND BIOMEDICINE

NOVA University Lisbon

March, 2023

DEPARTMENT OF LIFE SCIENCES

DECELLULARIZED FETAL SKELETAL MUSCLE AS AN *IN VITRO* SYSTEM TO STUDY A CONGENITAL MUSCULAR DYSTROPHY

ANA RITA GOMES SOARES

BSc in Biology

Adviser: Maria Gabriela Gomes de Figueiredo Rodrigues
Assistant Professor, FCUL Faculty of Sciences of the University of Lisbon

Co-advisers: Pedro Viana Baptista
Full Professor, NOVA School of Science and Technology

Examination Committee:

Chair: Ana Rita Fialho Grosso,
Assistant Professor, NOVA School of Science and Technology

Rapporteurs: Hélia Cristina Oliveira Neves,
Assistant Professor, Faculty of Medicine of the University of Lisbon

Adviser: Maria Gabriela Gomes de Figueiredo Rodrigues,
Assistant Professor, FCUL Faculty of Sciences of the University of Lisbon

MASTER IN MOLECULAR GENETICS AND BIOMEDICINE

NOVA University Lisbon
March, 2023

Decellularized fetal skeletal muscle as an *in vitro* system to study a congenital muscular dystrophy

ACKNOWLEDGMENTS

A realização desta tese foi um grande processo de aprendizagem, que não teria sido possível sem a ajuda de certas pessoas, às quais gostaria de expressar um especial agradecimento.

Em primeiro lugar quero agradecer à minha orientadora, Gabriela Rodrigues, por me ter proporcionado a oportunidade de trabalhar neste projeto. Agradeço por toda a sua disponibilidade, confiança e pelo apoio prestado, principalmente nesta última fase bastante intensiva da escrita.

Gostaria também de agradecer à Professora Sólveig Thorsteinsdóttir e à Professora Ana Rita Carlos, por me terem permitido fazer parte do grupo DEM e pelas suas partilhas de conhecimento.

Aos meus colegas e amigos de laboratório, Vanessa Ribeiro, Susana Martins, Inês Fonseca, Pedro Santos, Diogo Fernandes, Andreia Conceição, Claúdia Cavaco, Maria Neves, Ana Lopes, Catarina Melo, Hugo Luiz (são muitos e bons) por terem tornado os meus dias mais fáceis e mais divertidos, e por me terem apoiado não só no laboratório, como também por terem sido a minha grande massa adepta dentro dos relvados. Agradeço também ao Luís, à Marta Palma, ao Joaquim, à Rita Zilhão e ao Antonio Cordero.

Não poderia deixar de fazer agradecimento especial ao Pedro Santos, o grande mestre das descelularizações, por todo o carinho, paciência e por tudo aquilo que me ensinou ao longo desta jornada, sem ti este teria sido um trabalho bastante mais difícil.

Gostaria também de agradecer aos meus amigos de longa e curta data, por me animarem no contexto fora da faculdade. Por fim, um especial obrigado aos meus pais por estarem sempre presentes, por me apoiarem em todas as minhas decisões e por me terem tornado na pessoa feliz que sou hoje.

ABSTRACT

Laminin-α2-congenital muscular dystrophy (LAMA2-CMD) is caused by mutations in the *LAMA2* gene, which encodes for the α2 chain of laminin-211, a glycoprotein present in extracellular matrix (ECM). Studies in our laboratory using a mouse model of the disease (dy^{W} mice) have shown defects in fetal myogenesis.

To better understand the impact of both extracellular environment and the cellular niche during the onset of LAMA2-CMD, wildtype C2C12 myoblast (C2C12-WT) and *Lama2*-null myoblasts (C2C12-KO) were cultured in flasks and in decellularized fetal skeletal muscle obtained from embryonic day 18.5 healthy and $dy^{W-/-}$ fetuses.

Our findings suggest that the absence of laminin-α2 results in alterations in the expression levels of genes that encode for other ECM proteins. Additionally, our results also show that proliferation and differentiation are also affected. Indeed, although C2C12-KO cells cultured in decellularized matrices showed a higher expression level of *myogenin*, a differentiation marker, and a higher tendency to formed aligned cells in matrices, only C2C12-WT cells were able to fuse and form multinucleated myotubes.

The use of this novel 3D method allowed to reach a better understanding of the precise effects of laminin-α2 deficiency, which will be a requisite for the development of new therapies in the future.

Keywords: Laminin-α2-congenital muscular dystrophy, skeletal muscle, extracellular matrix, decellularization, myogenesis.

RESUMO

A distrofia muscular congénita laminina-α2 (LAMA2-CMD) é causada por mutações no gene *LAMA2,* que codifica a cadeia α2 da laminina, uma glicoproteína presente na matriz extracelular (ECM). Estudos no nosso laboratório usando o ratinho modelo (dy^{W}) para a doença LAMA2-CMD demonstraram defeitos na miogénese fetal.

Para entender melhor o impacto tanto do ambiente extracelular como das células no desencadear da LAMA2-CMD, mioblastos C2C12 selvagens (C2C12-WT) e mioblastos nulos para *Lama2* (C2C12-KO) foram cultivados em frascos e em músculo esquelético fetal descelularizado proveniente de fetos selvagens e fetos $dy^{W-/-}$ colhidos no estádio de 18.5 dias de desenvolvimento.

Os nossos resultados demonstram que a ausência de laminina-α2 resulta em alterações nos níveis de expressão de genes que codificam outras proteínas da ECM. Além disso, os processos de proliferação e diferenciação são também afetados. De facto, apesar das C2C12-KO cultivadas em matrizes descelularizadas exibirem um nível de expressão mais elevado de *miogenina*, um marcador da diferenciação, e uma maior tendência para alongar e alinhar, apenas as células C2C12-WT são capazes de fundir e formar miotubos multinucleados.

A utilização deste modelo 3D permitiu entender melhor os efeitos causados pela ausência de laminina-α2, o que poderá contribuir para o futuro desenvolvimento de novas terapias.

Palavras chave: Distrofia muscular congénita laminina-α2, músculo esquelético, matriz extracelular, descelularização, miogénese

CONTENTS

LIST OF FIGURES

LIST OF EQUATIONS

ABBREVIATIONS, ACRONYMS AND SYMBOLS

Arbp0	Acid ribossomal phosphoprotein PO
BM	Basement Membrane
BSA	Bovine Serum Albumin
C2C12-WT	C2C12 wild-type cells
C2C12-KO	*Lama2* knockout C2C12 cells
cDNA	Complementary DNA
CMD	Congenital Muscular Dystrophy
Ct	Cycle threshold
dECM	Decellularized extracellular matrix
DM	Differentiation Medium
DMEM	Dulbecco's Modified Eagle's Medium
DNA	Deoxyribonucleic Acid
DNase	Deoxyribonuclease
DTT	Dithiothreitol
E0.5	Embryonic day 0.5
E11.5	Embryonic day 11.5

E14.5	Embryonic day 14.5
E16.5	Embryonic day 16.5
E17.5	Embryonic day 17.5
E18.5	Embryonic day 18.5
ECM	Extracellular Matrix
EDTA	Ethylenediamine tetraacetic acid
FBS	Fetal Bovine Serum
GM	Growth Medium
HRP	Horse Radish Peroxidase
IM	Interstitial Matrix
JAK-STAT	Janus Kinase/Signal Transducers and Activators of Transcription
kDa	Kilodalton
LAMA2-CMD	Laminin-α2 Congenital Muscular Dystrophy
LB	Loading Buffer
MRF	Myogenic Regulatory Factors
MuSC	Muscle Stem Cell
MyoG	Myogenin
NT	Native Tissue
PBS	Phosphate-Buffered Saline
PCR	Polymerase Chain Reaction
Pen/Strep	Penicillin/Streptomycin
PFA	Paraformaldehyde
pH3	Phospho-Histone 3
rECM	Recellularized matrices

RT-qPCR	Real time quantitative PCR
SDS	Sodium Dodecyl Sulphate
SDS-PAGE	Sodium Dodecyl Sulphate-Polycrylamide Gel Electrophoresis
SM	Skeletal Muscle
TBST	Tris Buffered Saline 0,1% tween
TGF-β	Transforming Growth Factor-β
WT	Wild-Type
2D	Two Dimensional
3D	Three Dimensional

1

INTRODUCTION

1.1 Skeletal muscle and extracellular matrix

Skeletal muscle (SM) is a very dynamic tissue of the human body, accounting for about 40% of the total body mass [1]. It plays a crucial role in multiple functions such as movement, temperature regulation, glucose management, and storage of amino acids and carbohydrates [1], [2]. This tissue is characterized by a precise arrangement of muscle fibers and contains specialized stem cells known as muscle satellite cells [1], [2]. These cells, localized between the sarcolemma and the basement membrane (BM), play an important role in promoting muscle growth, repair, and regeneration [1], [3]. In addition to muscle fibers and satellite cells, the SM niche also comprises the extracellular matrix (ECM) (**Figure 1.1 A**).

The ECM is an important component of the muscle tissue and provides physical and biochemical support to the cells. It forms a non-cellular network that surrounds the muscle fibers and acts as a scaffold for cell adhesion, migration, proliferation, and differentiation [3]. The ECM not only provides physical support but also imparts mechanical properties such as tensile strength and contributes to the homeostasis and morphogenesis of the muscle tissue by releasing growth factors that are stored in the ECM network [4].

The ECM is an important component of the intramuscular connective tissue that can be classified in three independent and interconnected layers: epimysium (surrounding the muscle), perimysium (surrounding muscle fascicles), and endomysium (surrounding each muscle fiber) [3]. The endomysium shares a boundary with the myofiber sarcolemma at the BM (**Figure 1.1 B**).

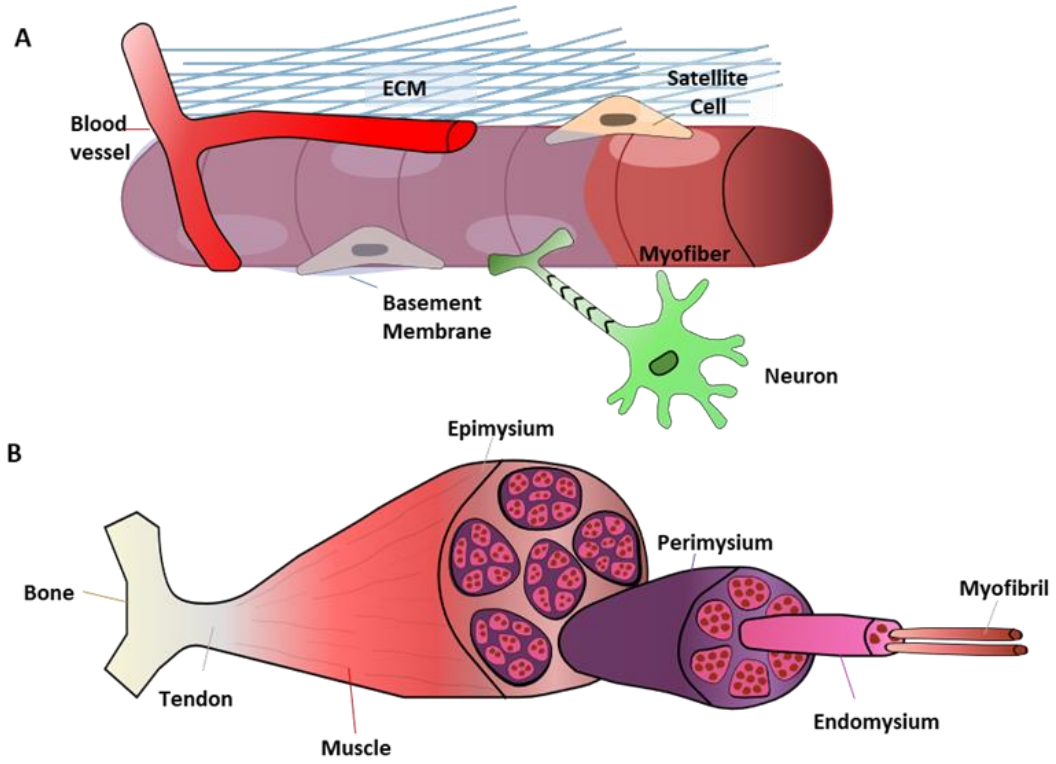

Figure 1.1 Skeletal Muscle Anatomy. **(A)** The satellite cell niche is a specialized microenvironment that comprises several components. Satellite cells reside between the basement membrane and the plasma membrane of myofibers. The extracellular matrix (ECM) plays a critical role in providing structural and signaling cues to the satellite cells. Blood vessels and nerves are also key components of this niche, as they provide nutrients, oxygen, and signaling molecules that regulate satellite cell behavior. Together, these components provide the necessary support and signaling cues for satellite cell maintenance, proliferation, differentiation, and self-renewal. **(B**) The musculo-skeletal system is made up of several components, including bone, tendon, nerves and blood vessels. The epimysium is a layer of tissue that surrounds the entire muscle, while the perimysium covers the fascicles within the muscle, and the endomysium encases each myofiber. Together, these layers of connective tissue provide structure and support to the muscle. (The figure is an original drawing of the thesis author using the VECTR - a free vector graphics editor)

The precise composition of ECM varies from tissue to tissue, but the main components of ECM include fibrous proteins such as collagen and elastins; proteoglycans; glycoproteins such as fibronectin and laminins; and specialized proteins, such as resident growth factors [4]. The dynamic structure of the ECM includes two distinct components that vary in structure and composition: 1) the interstitial matrix (IM) that surrounds cells and comprises a mixture of collagens, elastins, fibronectin and proteoglycans, and 2) the BM that is in close contact with cells and is composed of a mixture of proteins and glycoproteins, including collagens and laminins [5], [6] (**Figure 1.2**).

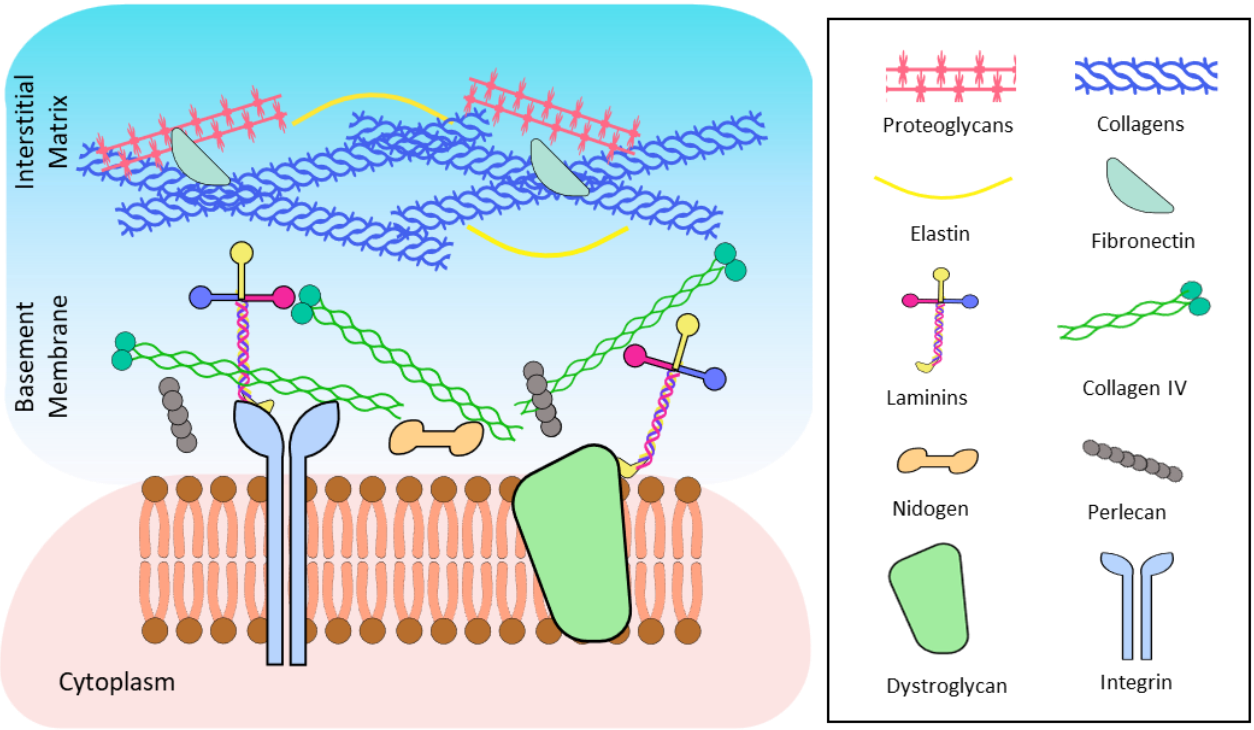

Figure 1.2. Extracellular matrix composition. The interstitial matrix constitutes by proteoglycans, collagens, elastin and fibronectin. The main components of basement membrane are laminins, collagen IV, nidogens and perlecan. These components contact with the cell via transmembrane receptors, like dystroglycan and integrins. (The figure is an original drawing of the thesis author using the VECTR - a free vector graphics editor)

1.2 Interstitial matrix and basement membrane

The IM fills the space between cells in tissues and organs and is linked by a network rich in collagen VI [7]. The IM encloses, separates, and supports the tissues [8]. It is primarily composed of a mixture of collagens, particularly collagen I and III, which provide tensile strength and interact with several proteins such as metalloproteinases, proteoglycans, and fibronectin [5]. IM also comprises fibronectin, which plays a crucial part in cell adhesion, proliferation, migration, and differentiation [5]. Elastin contributes to the tissue's elasticity, while hyaluronic acid is important for regulating tissue hydration and protecting the tissue by opposing compressional forces [8].

The BM is a sheet-like structure that is located beneath the epithelial and endothelial cells, among others, and provides structural support, controls cell organization and differentiation,

and interacts with cell surface receptors [5], [9]. BM starts to form early in embryonic development, and is composed of collagen, laminins, nidogen and perlecan (a heparan sulfate proteoglycan) [10] (**Figure 1.2**).

Collagens are the most prominent ECM component in SM as they play a crucial role in the regulation of cell attachment and differentiation, providing tensile strength to bones. Collagen type IV, a triple-helical molecule, is a nonfibrillar collagen that makes up about 50% of all BM [10]. The collagen network is covalently linked together by multiple chemical bonds that are thought to confer the tensile strength of the BM [11]. Collagens type VI and type VIII are also associated with the BM [5].

Laminins are the most abundant non-collagenous glycoproteins present in BM [10]. They are composed of a combination of three chains (α, β and γ) which exist in different forms, forming at least 16 different laminins [7]. In mature SM, laminins containing the α2 chain are the main component of the BM, with laminin-211 (α2 β1 γ1) being the major form around the sarcolemma of mature myofibers, whereas laminin-221 (α2 β2 γ1) occurs at myotendinous and neuromuscular junctions [7]. Laminins have a dual function in both scaffolding and signaling [8]. Their N-terminal domain interacts with several biomacromolecules of the BM, defining the BM's architecture [8]. On the other hand, their C-terminal domain binds to cell surface receptors, including integrins and the dystroglycan protein complex, thus creating a link between the ECM and the muscle cell cytoskeleton [8].

Laminins and collagen type IV individually self-assemble into suprastructures and create a network that is crucial for BM stability [11]. Nidogen and perlecan, due to their high affinity for both laminin and collagen, can bind to these molecules and increase the stability and influence the structural integrity of BM [10]. BM is also includes other components such as the proteoglycan agrin, the glycoprotein fibulin, and the collagen-binding matricellular protein [10].

1.3 Skeletal muscle development and extracellular matrix contribution

In vertebrates, the SM of the trunk and limbs is formed from somites present in the paraxial mesoderm. The initial immature somites are surrounded by a fibronectin-rich matrix that allows the formation of somite boundaries during somitogenesis and also participates in the

maintenance of the epithelial organization of somitic cells [12], [13]. As segmentation begins, a new BM constituted by laminin-111 and -511, collagen IV, and perlecan is deposited around each newly-formed somite [12], [14]. After their formation, the somites undergo a maturation process that originates different compartments. In the ventral region, the somites de-epithelialize, BM disintegrates and the sclerotome is formed, which will provide the cells for the vertebrae and ribs. The somites present in the dorsal zone remain epithelial and constitute the dermomyotome, which gives rise to all trunk, limb, and a few head muscles, as well as some dermal, endothelial, smooth muscle and brown fat precursors [14].

In the dermomyotome, the somitic BM does not disintegrate and remains tightly associated with the basal side of the dermomyotome, which prevents a precocious myogenic differentiation [12], [14]. As the dermomyotome grows progressively through symmetric divisions, the muscle stem cells (MuSCs) from the dermomyotome edges delaminate and then migrate underneath to form the myotome - a transient structure that will be transformed into deep back muscles (epaxial part) and into intercostal, body wall and limb muscles (hypaxial part) [15], [16].

During myotome formation, the cells that delaminate from the dermomyotome are Pax3 and/or Pax7-positive cells [17]. Pax3 and Pax7 are transcription factors that are involved in the activation of myogenic regulatory factors (MRFs), the ones which will induce myogenesis. In vertebrates there are four MRFs named the myogenic factor 5 (Myf5), the myogenic factor 6 (Myf6, also known as Mrf4), the myogenic differentiation 1 (MyoD) and myogenin [18]. When an embryonic MuSC starts the expression of Myf5, Mrf4 or MyoD, it becomes committed to myogenesis and is termed a myoblast. These myoblasts proliferate a few times and then start expressing myogenin, which induces their exit from the cell cycle and their terminal differentiation into myocytes. The myocytes start to elongate and synthesize muscle structural proteins such as desmin and myosins [19] (**Figure 1.3**).

The myotomal myogenesis begins at embryonic day (E) 9.5 and, as the cells enter the myotome, a new BM is formed between the myotome and the sclerotome [12]. The main role of this myotomal BM is to create a physical barrier between the myotome and sclerotome that thus helps the patterning of the myotome [12]. As the myotome grows, the number of myoblasts and myocytes increases and their interaction with the matrix changes [20], [21]. Newly arrived cells are found closer and assemble to the BM and do not proceed in the differentiation process until they reach the central region of the myotome, where the membrane is discontinuous, and

where they begin to express myogenin, allowing the elongation of myotomal myocytes [21]. In this way, the BM, in addition to forming a barrier, is still important for the migration and elongation of cells and essential for cell fate and differentiation [12]. At E11.5 the myotomal BM starts to disintegrate and the myotome disappears as a segmented structure.

Primary or embryonic myogenesis provides the basic muscle pattern of the body and starts in mouse at E11.5 and ends around E14.5 [14]. In this stage, Pax3 and/or Pax7 positive cells differentiate into primary myoblasts and start to fuse with the elongated myocytes and/or with each others to form the primary multinucleated myotubes (**Figure 1.3**). These primary myotubes attach to the tendons by E14.5 and are innerved by motor neurons. During primary myogenesis, the laminins and other components of myotomal BM are disassembled, this process being laminin-independent [20], [22].

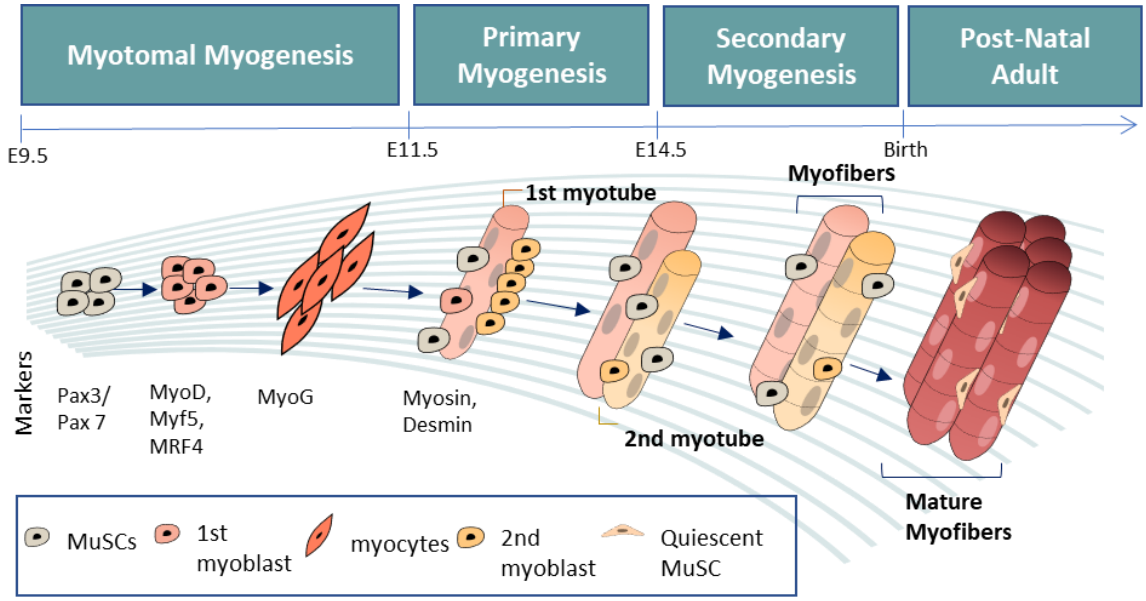

Figure 1.3. Skeletal Muscle Development. The myogenesis begins with the delamination and migration of MuSCs, expressing Pax3 and Pax7, from the dermomyotome to the myotome. Once in the myotome, the MuSCs are induced to differentiate into myoblasts and begin expressing MRFs, such as MyoD and Myf5. After dividing a few times, the myoblasts start to express myogenin (MyoG) and differentiate into myocytes. During primary myogenesis, the myocytes start to fuse with each other to form primary multinucleated myotubes, that express myosin and desmin. In secondary myogenesis, proliferative MuSCs differentiate into secondary myoblasts and fuse with the primary myotubes to generate secondary myotubes. The ongoing addition of new myotubes, along with the fusion of myoblasts, results in the growth of skeletal muscle. In post-natal development, myotubes mature into myofibers and MuSCs became quiescence cells, allowing muscle growth and regeneration. (The figure is an original drawing of the thesis author using the VECTR - a free vector graphics editor)

Between E14.5 and until birth, secondary or fetal myogenesis occurs, where the MuSCs that did not differentiate during primary myogenesis become committed myoblasts, differentiate, and, using the primary myotubes as scaffolds, fuse to each other giving rise to secondary myotubes [14]. The secondary myoblasts also fuse with the existing primary myofibers, increasing their size. In this way, skeletal muscle growth occurs by hyperplasia - through the addition of new myotubes and by cell-mediated hypertrophy - through the fusion of myoblast to existing myofibers [22].

As the fetal myogenesis begins, laminins-211, -411 and -511 start to assemble around the myofibers. By E16.5, Pax7-positive MuSCs enter the space between the myofiber and its BM, and establish their niche [22]. During peri- and postnatal development, MuSCs divide and differentiate to continue muscle growth. These MuSCs then enter a quiescent state and become satellite cells, which are responsible for postnatal growth, muscle regeneration, and hypertrophy [15], [23].

1.4 Extracellular matrix defects and muscular dystrophies

Normal SM function depends not only on the functional integrity of myofibers and sarcomeres but also on a structural and functional ECM [24]. As mentioned above, the muscle ECM plays an important role in giving structural support, allowing the migration, proliferation, and differentiation of stem cells and it is also paramount in the regulation of growth factors activity. Due to its importance, mutations in skeletal muscle ECM and basement proteins can cause muscle disease, such as muscular dystrophy [24]. Muscular dystrophies are inherited myogenic disorders characterized by progressive muscle weakness and loss of muscle mass with varying levels of severity [25]. The mutations result in the absence or expression of truncated forms of important muscle proteins [26]. These proteins are unable to form functional protein complexes and the linkage ECM-to-receptor-to-cytoskeleton is compromised, leading to myofiber fragility and, consequently, progressive muscle weakness [26], [27]. There are many muscular dystrophies associated with ECM. For example, mutations in the dystrophin-glycoprotein complex, which links ECM to the cytoskeleton, cause Duchenne-type [28]. Defects in BM associated proteins such as laminin and collagen VI leads to congenital muscular dystrophy and Ullrich/Bethlem diseases, respectively [28].

1.5 LAMA2-Congenital muscular dystrophy

Congenital muscular dystrophies (CMD) are rare types of muscular dystrophies that occur at birth or early during infancy [25]. Laminin-α2-congenital muscular dystrophy (LAMA2-CMD), also referred to as merosin deficient muscular dystrophy, is one of the most common congenital muscular dystrophies in the world, representing 36.4%-48% of CMD patients. This autosomal recessive disease occurs due to mutations in the *LAMA2* gene, which encodes for the α2-chain present in laminin-211 and -221 [29].

While laminin-211 is the major form of laminin around the sarcolemma of mature myofibers, laminin-221 is found in neuromuscular junctions [26]. Together these types of laminins are the main isoforms present in adult SM [30]. Laminin-211 and -221 are the major ligands of cellular receptors such as α7β1 integrin and α-dystroglycan [30]. Therefore, the absence of functional laminin leads to the disruption between the ECM and the cytoskeleton, triggering a cascade of secondary problems such as cell membrane instability, apoptosis and necrosis of muscle fibers, inflammation and fibrosis [30], [31] (**Figure 1.4**). Furthermore, these laminins are also expressed in Schwann cells, and therefore, mutations in the α2 chain lead to reduced myelination resulting in impaired conduction velocity and peripheral neuropathy [26].

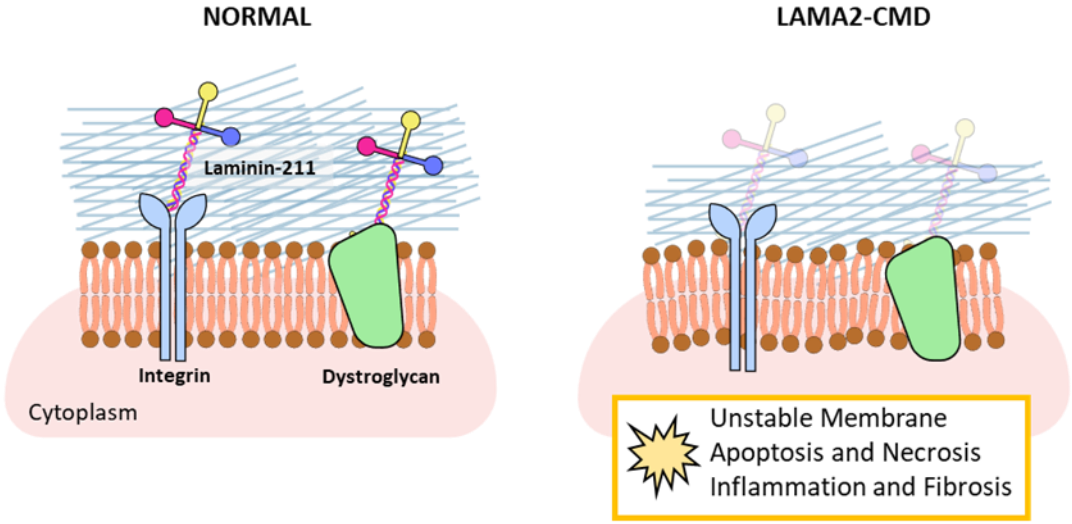

Figure 1.4 Molecular model in a normal and laminin-α2-deficient patient. In normal conditions, laminin-211 binds to ECM proteins and to muscle cell receptors such as integrin-α7β1 and α-dystroglycan protein complexes. In LAMA2-CMD, there is no functional laminin-α2 and the link between the ECM and cytoskeleton is disturbed, which can trigger a cascade of negative effects. These may include destabilization of the cell membrane, muscle fiber apoptosis and necrosis, inflammation and fibrosis. (The figure is an original drawing of the thesis author using the VECTR - a free vector graphics editor)

The clinical spectrum of LAMA2-CMD varies from a severe phenotype, in approximately 90% of the cases, to a mild phenotype. Severe phenotypes are associated with a complete absence of laminin-α2 and are due to homozygous or bi-allelic loss-of-function mutations [24]. Disruptions can occur at both the N-terminal and C-terminal of laminins, affecting their self-assembly and their capacity of assemble with other proteins, as well as preventing cell receptor binding, respectively [24], [30]. In the severe phenotypes, patients show symptoms from birth and these include hypotonia, muscle weakness and progressive muscle wasting [32]. Most patients do not achieve ambulatory independence and show progressive joint contractures, feeding problems and respiratory insufficiency, with the latter being the main cause of death [32]. Some patients also exhibit seizures and mental retardation [27].

Mild phenotypes are associated with other types of mutations such as missense or frameshift mutations, which result in a small reduction in laminin-α2 expression [27]. This phenotype is characterized by a slower progression of the disease, with the first symptoms occurring later during childhood. Despite the delayed motor milestones, patients are able to achieve ambulatory independence [32]. Since laminin-α2 is also expressed in the central nervous system, peripheral nervous system and the heart, these tissues are also affected in both phenotypes [29]. Unfortunately, to date, there is no cure for this disease and the therapeutic approaches are limited to alleviating the symptoms [26].

Currently, there are several mouse models used to study LAMA2-CMD, including dy^{2J}/ dy^{2J}, dy^{3K}/dy^{3K} and dy^{W}/dy^{W} ($dy^{W-/-}$), with the latter being the most characterized and widely used model [27]. The $dy^{W-/-}$ mouse was generated by homologous recombination and expresses a small amount of truncated α2 chain lacking the N-terminal domain [29], [33]. This mouse has a severe phenotype characterized by muscle fiber loss, inflammation, fibrosis, impaired muscle function, and peripheral neuropathy, and typically dies 5-12 weeks after birth [33].

1.5.1 LAMA2-CMD *in utero*

Using the $dy^{W-/-}$ mouse model it was possible to realize for the first time that the onset of LAMA2-CMD begins *in utero*, more specifically during the final stage of secondary myogenesis [22]. As previously mentioned, during secondary myogenesis the BM (consisting mostly of

laminins) starts to assemble around the myofibers [19]. Nunes *et al.* detected that in the absence of laminin-α2, the end of this phase, more precisely between E17.5 and E18.5, is marked by defects that include a decrease in the number of Pax7 and myogenin-positive cells [22]. Furthermore, although $dy^{W-/-}$ mice have a normal number of myofibers, the muscles are significantly smaller and show impaired muscle growth that does not recover postnatally [22]. Together these data suggest that the $dy^{W-/-}$ mouse is unable to produce enough MuSCs that allow fetal myofiber growth in normal conditions.

The stem cells are present in a complex three-dimensional (3D) microenvironment, referred to niche, which provides crucial extracellular signals for the survival and maintenance of stem cell identity [33]. During embryonic and fetal development the MuSCs amplification occurs *via* symmetric divisions, where a Pax7 positive cell originates two identical Pax7 positive cells [34]. This type of division is promoted by the contact of the cells with the myofibers and the ECM [35]. During these stages, the BM seems to maintain cells in a non-committed state [21]. Therefore, to maintain the self-renewal of MuSCs the presence of a functional 3D matrix is essential [22]. Alternatively, the stem cells can also divide by asymmetric divisions originating an identical Pax7 positive cell and a committed cell which will later differentiate and fuse with the muscle fiber [22], [35]. This type of division is more common after birth and allows the maintenance of the stem cell pool [19], [35].

In the niche, accurate balancing of symmetric and asymmetric cell divisions is crucial for preserving an adequate number of stem cells and meeting the demands for differentiated cells in the neighboring tissues [36]. Disruption in the muscular niche can negatively affect SM development. Indeed, Nunes *et al.* found that during secondary myogenesis the lack of functional laminin-221 triggers activation of the JAK-STAT pathway, altering the balance of symmetric and asymmetric divisions. This shift from symmetric to asymmetric divisions reduces the number of Pax7-positive cells, which are required for fetal muscle growth [22].

Our research group has been focusing on uncovering the molecular and cellular processes involved in the onset of LAMA2-CMD. In order to understand the underlying mechanisms and the matrix properties that can influence this disease, it is important to examine the interactions between cells and the matrix [37], [38].

1.6 C2C12 cells as an *in vitro* model

Immortalized cell lines have proven valuable for investigating cellular processes and disease mechanisms, given the difficulty of accessing primary cells. C2C12 is a well-established myoblast cell line derived from mouse SM satellite cells, which can proliferate easily in a serum-rich medium and undergo spontaneous differentiation upon serum removal [39], [40]. Due to its similarity to activated satellite cells, C2C12 myoblasts are frequently used in studies of myogenic processes [40]. Our research group established a *Lama2*-null C2C12 (C2C12-KO) cell line to use as an *in vitro* model for investigating the mechanisms underlying LAMA2-CMD [41]. This model will be used in this thesis to determine whether laminin-α2 deficiency affects cell proliferation and differentiation in the context of the disease.

In vitro systems provide a controlled environment that enables the study of cell behavior, drug actions, and the engineering of tissues. Two-dimensional (2D) *in vitro* models are very useful due to ease of manipulation, cost-effectiveness, and ability to reduce the use of laboratory animals [42]. However, the fact that cells are grown in monolayers on plastic dishes leads to several drawbacks. The 2D systems do not mimic the natural structure of tissues and hinder cell-cell and cell-extracellular environment interactions, which are critical for understanding the biological processes *in vivo* [42]. Recently, there has been a growing interest in 3D *in vitro* models, such as decellularized scaffolds seeded with stem cells, for both basic research and clinical studies. These 3D models are capable of preserving the main molecular and mechanical properties of native tissues and have been employed to create functional organ mimetics [38].

1.7 Decellularization of skeletal muscle

Decellularization is a technical process that involves removing cellular components from tissues or organs while preserving the biochemical, physical, and mechanical features of the NT ECM [43]. The decellularization process involves diverse approaches such as physical and chemical agents, enzymes, detergent solutions, or a combination of these [43].

In the last decade, an increasing number of protocols have been developed and modified for decellularizing SM [44]. Sodium dodecyl sulphate (SDS) and triton-X-100 are detergents that have been used to decellularize SM, which act by destabilizing cell membranes, causing cell lysis [43], [44]. However, high concentrations or prolongated exposure to SDS can also disturb

the molecular organization of the BM [43], [45]. As the ECM plays a critical role in SM, preserving its components after the decellularization process is crucial [44], [46]. Therefore, it is essential to ensure that SM decellularization protocols assure a balance between removing cellular content and preserving ECM components.

The preservation of the native ECM composition and architecture promotes cell adhesion, proliferation, migration, and differentiation [46]. As a result, decellularized matrices (dECM) have a wide range of applications. Currently, decellularized SM has been used as a scaffold for engineering muscle graft implants to facilitate regeneration after injury [46]. However, dECMs can also be used as powerful *in vitro* tools to study drug responses, disease phenotypes, and cell-matrix interactions [46].

Our research group is interested in understanding the cellular and molecular processes involved in the onset of LAMA2-CMD. To this end, we recently developed a new 3D *in vitro* model based on the decellularization of fetal SM [45]. Deep back muscles from E18.5 fetuses were isolated and treated with a hypotonic buffer, SDS, and DNase [45]. The E18.5 stage was chosen because it corresponds to the earliest manifestation of LAMA2-CMD [22]. The ECM characterization using immunostaining and western blot techniques showed that the main ECM proteins were preserved, and DNA quantification revealed an almost complete absence of DNA in dECMs compared to the NT, indicating the success of this decellularization protocol. When the dECM were recellularized with C2C12 myoblasts, cells were able to adhere, proliferate and differentiate, indicating the suitability of these scaffolds as a model system for the 3D culture of cells [45]. This *in vitro* model can therefore be used to study the interactions between muscle cells and the fetal ECM and can be a game changer for unravelling the mechanisms involved in LAMA2-CMD and developing potential new therapies.

1.8 Aims of this thesis

The objective of this thesis is to optimize the 3D *in vitro* model for studying the interactions between the extracellular and the cellular niche, specifically in the context of LAMA2-CMD. To achieve this, we will characterize the ECM after the decellularization of fetal SM. Different combinations of matrices and cells will be generated to determine whether the absence of laminin-α2 affects cell-matrix interactions on the onset of LAMA2-CMD. The wildtype (WT) dECM will

be recellularized with C2C12-WT myoblasts (WT x WT) and with C2C12-KO cells (WT x KO). The same will be applied to *dy*$^{W-/-}$ dECM, giving rise to the combinations *dy*$^{W-/-}$ x WT and *dy*$^{W-/-}$ x KO. Apart from the 3D model, we will also use an *in vivo* WT and *dy*$^{W-/-}$ deep back muscles and a 2D *in vitro* model where C2C12-WT and C2C12-KO cells will be cultured in flaks. These models will be compared to understand whether the absence of laminin-α2 affects the composition of the ECM, and the proliferation and differentiation properties of the cells. Additionally, we aim to determine whether the presence of functional laminin-α2 in either the extracellular matrix or the cells can counteract the effect of the disease.

2

MATERIALS AND METHODS

2.1 Mouse model and fetus collection

All the research procedures performed were approved by the Animal Welfare Committee (ORBEA) of the Faculty of Sciences, University of Lisbon, and Direção Geral da Alimentação e Veterinária (DGAV; ref. 0421/000/000/2022) and are in accordance with the European Directive 2010/63/EU.

In this thesis, the genetically modified *dy*$^{W-/-}$ mouse, which is the most widely used model to study LAMA2-CMD pathogenesis, was used. Mutants homozygous animals of this strain only produce a truncated form of the laminin-α2, which is nonfunctional due to the presence of a LacZ-neo cassette that was inserted into the *LAMA2* gene [47].

E18.5 homozygous *dy*$^{W-/-}$ and WT fetuses were obtained by crossing heterozygous *dy*$^{W+/-}$ mice. The breeding confirmation was performed in the morning of the following day (E0.5), by the presence of a white vaginal plug. Pregnant females were identified by small lateral bulges and by their pear-shaped appearance. Subsequently, the females were anesthetized via isofluorane inhalation and sacrificed by cervical dislocation.

The E18.5 fetuses were removed from the uterine horns, immersed in ice-cold phosphate-buffered saline (PBS), and sacrificed by decapitation. The tails were removed for genotyping. The deep back muscles were isolated and used in the experiments. For short-term preservation, muscles were stored at 4 °C in PBS. For long-term preservation, muscles were kept at -80 °C.

2.1.1 Genotyping

For genotyping, the tails that were cut from each fetus were placed into a microcentrifuge tube. Next, 25 mM NaOH / 0.2 mM EDTA was added to each tube and heated in a thermocycler at 95°C for 30 minutes (min). Then, the tubes were cooled to 4°C and 40 mM Tris HCl was added in a 1:1 ratio to the mixture. For polymerase chain reaction (PCR), 1 µL of the mixture was used per PCR tube. All PCR reactions were performed using Xpert Fast Hotstart DNA Polymerase. To perform genotyping of $dy^{W-/-}$, a single mix was prepared with the three primers (Annexes Table A.1). PCR was performed according to the protocol in Annexes Table A.2.

2.2 Tissue decellularization

After collection, each piece of deep back muscle was added to a 12 multi-well and submitted to the decellularization protocol. The decellularization protocol consists of a 3-day protocol with successive washes and includes 3 steps: cell lysis by osmotic shock with hypotonic buffer, plasma membrane dissolution and protein dissociation with 0.05% SDS, and enzymatic destruction of DNA with DNase treatment. All the procedures were performed in a laminar flow hood and under sterile conditions.

The protocol was performed as described in Gameiro dos Santos *et al.* [45]. Briefly, on day one, each piece of epaxial muscle was washed with 1x PBS to remove eventual residual blood and then incubated with 3 mL of hypotonic buffer (1.21 g Tris Base, 1 g EDTA, filled to 1 L distilled water, pH adjusted to 7.8) for 18 hours. On the next day, the samples were washed three times with 3 mL of PBS (1 hour per wash) and then incubated for 24 hours with 3 mL of 0,05% SDS diluted in hypotonic wash buffer (1.21 g Tris Base, filled to 1 L distilled water pH adjusted to 7.8). On the last day, the tissue fragments were submitted to three washes of 20 min each with 3 mL of hypotonic wash buffer and then incubated for 3 hours with 2 mL of DNase treatment (1.21 g Tris Base, 1 mL 1M MgCl2, filled to 0.5 L distilled water, pH adjusted to 7.8) at 37 °C. After this period the samples were washed 3 times for 20 min each with 1x PBS. A last wash was performed overnight under agitation (2 *g*). All the steps, were performed under agitation (18 *g*) at 25 °C, unless otherwise stated, and all solutions contain 1% Penicillin (10000U/ml)/Streptomycin (10 mg/ml) (Pen/Strep).

The dECM were then maintained at 4 °C in PBS 1 x until recellularization or stored at -80 °C for other experiments.

For more details about the decellularization protocol see [45].

2.3 *In vitro* procedures

2.3.1 Cell culture – 2D approach

We used a well-established myoblast cell line (C2C12-WT) and a *Lama2*-null cell line (C2C12-KO) that was previously generated in the host laboratory to mimic LAMA2-CMD. The C2C12-KO was generated with a CRISPR-Cas9 vector targeting the *Lama2* gene. For more details about the establishment of *lama2-null* cell line see [41]. C2C12-WT and C2C12-KO myoblast were grown in Dulbecco's modified medium (DMEM) supplemented with 10% fetal bovine serum (FBS) and 1% Pen/Strep. The cell lines were maintained in a 5% CO_2 atmosphere, with constant humidity and at 37℃. When ~70% of confluency was reached, the cells were washed twice with 1x PBS and 0.05% Trypsin/0.53 mM EDTA was used to pass the cells. The culture medium was replaced every two days.

2.3.2 Recelullarization - 3D approach

After decellularization, the matrices can be recelullarized. Before this process, the WT and *dy*$^{W-/-}$ dECM were first cut into pieces of approximately 500 µm x 500 µm x 200 µm. Each piece was placed in a 96 multi-well (maximum 3 pieces per well) and growth medium (DMEM supplemented with 10% FBS and 1% Pen/Strep) was added. The dECM were placed in culture medium in an incubator at 37 °C for 2 hours for the dECM to absorb the growth medium.

For the recellularization process, we used C2C12-WT and C2C12-KO cells. The cells were first washed twice with 1x PBS solution and then detached from the culture dish using 0.05% Trypsin/0.53 mM EDTA. After counting the cell suspension with a hemocytometer, 50,000 cells in fresh 200 µL growth medium were added to each well, after removing the culture medium from the 96 multi-well plate with the dECMs. The matrices and cells were maintained in the 96 multi-well for two days to allow cell adhesion to the matrix. After two days, the recellularized

matrices (rECM) were transferred to a 48-well plate and the culture medium was changed every two days.

Depending on the type of experiment the rECM were maintained in culture for 8 or 12 days in growth medium. For the differentiation process to be induced, after a period of 8 days, the growth medium was replaced by the differentiation medium (DMEM supplemented with 2% horse serum and 1% Pen/Strep) and the culture can be extended for another 4 or 7 days.

All the procedures were performed in a laminar flow hood and under sterile conditions.

2.4 Real Time-qPCR

2.4.1 RNA extraction

C2C12 cells were lysed in 500 µL of TRIzol reagent. The deep back muscles, which were previously isolated from fetuses and stored at -80 °C, and the rECM maintained in culture for 8 days were homogenized in 500 µL of TRIzol using a tissue homogenizer. Following the dissociation of nucleoprotein complexes, 100 µL chloroform was added to each sample and the mixture was centrifuged for 15 min at 12,000 *g* at 4 °C to separate the mixture into three phases: a lower red phenol-chloroform, an interfase, and a colorless upper aqueous phase that contained the RNA. The aqueous phase was transferred to a new tube, and 250 µL of isopropanol was added to precipitate the RNA. After 10 min of incubation on ice, the samples were centrifuged for 10 min at 12,000 *g* at 4 °C. The supernatant was discarded, and the pellet was washed twice in 500 µL of 75% ethanol and then centrifuged for 5 min at 7,500 *g* at 4 °C. The ethanol was removed, and the pellet was air-dried. The pellet was resuspended in 20-50 µL of RNase-free water, placed on ice, and incubated for 10 min at 55 °C. RNA concentration and quality were determined using a Nanodrop 1000.

2.4.2 cDNA and RT-qPCR

Complementary DNA (cDNA) was produced from the single-stranded RNA obtained in the previous RNA extraction step, using the Xpert cDNA Synthesis Kit. The reaction mixture consisted of 1 µl of deoxynucleotide triphosphate mix, 1 µl of random hexaprimer, RNase-free

water, and 1 µg of RNA. The addition of 4 µl of 5X reaction buffer, 0.5 µl of RNase inhibitor (40 U/µl), and 1.0 µl of Xpert RTase (200 U/µl) completed the mixture. The solution was then mixed and run through a thermocycler at 25 °C for 10 min, 50 °C for 50 min, and 85 °C for 5 min. The resulting cDNA was stored at -20 °C for future real time quantitative PCR (RT-qPCR) analysis.

For the RT-qPCR reaction, a SsoAdvanced Universal SYBR Green Supermix was used. The reaction mixture consisted of 9 µl per reaction, which included 5 µl of Universal SYBR Green Supermix (2x), 0.4 µl each of forward and reverse primers, and 3.2 µl of nuclease-free water. All components were properly mixed and distributed in each well of 96 multi-well. All primer sequences used are listed in Annexes Table A.3. Then 1 µL of cDNA was added to each well containing the reaction mix. The plate was sealed with an optically transparent film and centrifuged to remove air bubbles and to ensure that the mixture remained at the bottom of each well. In the end, the plate was placed in the CFX96TM Real Time PCR Detection System with the protocol in Annexes Table A.4. Data analysis of the PCR run was performed by analyzing the threshold cycle (Ct) values and comparing the Ct value of the gene of interest (GOI) and the housekeeping gene, according to the following equations:

Equation 2.1

$$\Delta Ct = CT_{housekeeping} - CT_{GOI}$$

Equation 2. 2

$$\text{Fold difference to housekeeping} = 2^{\Delta Ct}$$

The quality of all PCR reactions was assessed by melting curve analysis.

2.5 Western blot

2.5.1 Protein extraction

Native tissue (NT) and dECM from WT and *dy*$^{w-/-}$ fetuses previously frozen at -80 °C were added to a tube containing 2x sodium dodecyl sulphate-polyacrylamide gel electrophoresis (SDS-PAGE) loading buffer (LB) with 100 mM dithiothreitol (DTT). The protein extraction was made directly in LB, to avoid protein loss. Samples were then homogenized in a tissue lyser, incubated

in a thermomixer for 10 min at 50 °C and centrifuged for 10 min at 10,000 *g* at 4 °C. Finally, the supernatant was transferred to another tube and protein concentration was measured using Nanodrop 1000. The samples were stored at -20 °C to further use.

2.5.2 Western blot

Since the proteins under analysis have a high molecular weight (120-400 KDa), a precast acrylamide gradient gel was used (4% - 20%). 100 µg of the protein and 10 µL of high molecular weight protein standard were loaded. Then the samples were electrophoresed in 1x Running Buffer (14.42 g Glycine, 3.02 g Tris, 1 g SDS, filled to 1 L distilled water) for 10 min at 150 V and then 70 min at 175 V, using an electrophoresis system.

After electrophoresis, the gel and the activated polyvinylidene fluoride membrane were mounted in a transfer cassette and transferred in chilled transfer buffer (5.82 g Tris, 2.93 g glycine, 200 mL of methanol, up to 1 L distilled water) on a bed of ice for 90 min at 100V. The quality of the transfer was then assessed by a Coomassie blue substitute.

The membranes were blocked for 1 hour in 5% powdered milk in TBST (20 mM tris, 150 mM NaCl, 0.1 % tween20 and distilled water, pH 7.4-7.6), under agitation. The membranes underwent three rinses with TBST and were then treated with the primary antibody that was diluted in a solution of 2% bovine serum albumin (BSA) and 0.02% sodium azide in TBST. This incubation took place overnight at 4 °C with agitation, and the information regarding the antibodies and dilutions used can be found in Annexes Table A.5. On the next day, the membranes were washed for 5 min with TBST and incubated with horse radish peroxidase (HRP)-conjugated secondary antibodies (diluted in TBST with 5% milk) for 1 hour at RT. The membranes were then washed three times for 10 min with TBST. The detection of chemiluminescence was performed using a commercially available developing kit. The images were captured using the Amersham Imager 680 RGB.

2.6 DNA quantification

For the quantification of DNA, it is necessary to calculate the wet weight of the sample. We did that by weighing an empty Eppendorf tube and then the same tube with the NT or dECM sample. Sample weight is calculated by the following equation:

Equation 2.3

$$\text{Sample wet weight} = \text{weight}_{\text{tube with sample}} - \text{weight}_{\text{empty tube}}$$

A spin-column kit was utilized for extracting DNA from both NT and dECM samples. A digestion buffer was added to each sample, which was then homogenized using a bead mill according to the manufacturer's instructions (DNeasy Blood & Tissue Kit). Next, proteinase K was added to each sample and incubated overnight at 56 °C with slow agitation. The manufacturer's buffer was then eluted and the samples were centrifuged to enhance the DNA yield. The DNA present in the samples was quantified using a fluorescent double-stranded DNA detection kit. Finally, the DNA content was normalized to nanograms per milligram of the original wet weight of the sample.

2.7 Immunohistochemistry

After reaching the desired timepoint, the rECM WT and *dy*$^{w-/-}$ were washed with 1x PBS for 10 min to remove the culture medium, followed by fixation in 4% paraformaldehyde in PBS for 2 hours at RT and under agitation. After this time, rECM were washed with PBS and permeabilized with 0.2% triton-X100 in PBS for 20 min and washed again with PBS. Then, rECM were blocked with blocking solution (1% BSA, 1% goat serum, 0.05% triton-X100 in PBS) for 1 hour at RT. All the procedures were performed under agitation. Finally, the rECM were incubated with the primary antibody diluted in blocking solution overnight at 4 °C.

The next day, rECM were washed three times 10 min with PBS and incubated with secondary antibody, methyl green and phalloidin diluted in blocking solution for 1 hour at RT. After this time, rECM were washed twice with 4x PBX for 10 min and the nuclei were stained with DAPI

(4',6-diamidino-2-phenylindole) for 30 seconds. Samples were then mounted in anti-fading medium (50 mg/ml propyl gallate in PBS:glycerol, 9:1) between 2 coversplips separated by steel rings and glued together with bee wax. 100 µM image stacks were then acquired in a Leica SPE confocal microscope system.
All antibodies and dyes, and the respective dilutions, are listed in Annexes Table A.5.

2.8 Cell viability assay

To analyse cell proliferation, the resazurin assay was performed. For that, each rECM was transferred to a 96 multi-well plate with 100 µL culture medium with 0.1% resazurin and were incubated for 4 hours at 37 °C (one rECM per well). After this time, the rECM were placed back in the initial 48 multi-well plate and the 100 µL of medium with resazurin was collected to a reading plate. Fluorescence levels (excitation filter 531/40 nm; emission filter 595) were then measured using Victor 3V plate reader.

The resazurin assay was performed at day 4, 6, 8 and 12 of culture, both in cells cultured in growth medium and in differentiation medium (starting on day 8). After reading, fluorescence values were normalized using a cell-free matrix sample. Each sample was composed of 3 replicates. To analyze proliferation the normalized values were divided by the first day of the assay (day 4 of culture).

2.9 Image analysis and quantifications

Fiji software was used to process and analyse all images. Confocal image stacks of 100 µm were compressed into one maximum intensity projection image resorting to the Maximum Intensity Z-projection Plugin in Fiji.

To quantify the number of phospho-histone 3 (pH3)-positive cells, the rECM were immunostained for pH3 and counterstain with methyl green, to detect the total number of cells. Total cell and pH3-positive cell quantification was performed manually using Fiji Puglin Cell Counter (**Figure 2.1**). The ratio was obtained by dividing the number of positive cells for pH3 by the total number of cells stained with methy green present in each rECM.

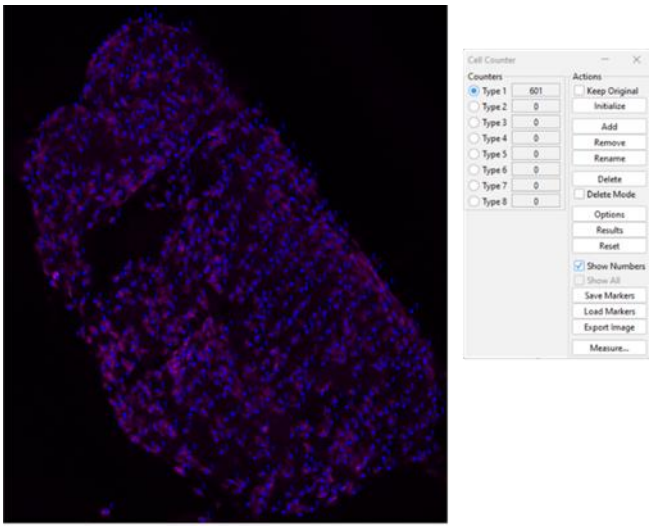

Figure 2.1 Cell counter window of Fiji software. Nuclear staining with methyl green was used to count the number of cells. Each blue dot represents an individual cell. The figure depicts a recellularized WT matrix with C2C12-KO cells, which were cultured for 8 days in growth medium.

2.10 Statistical analysis

All statistical analyses were performed using GraphPad Prism 8.0.2 program. A Student's t-test was used to test for differences between mRNA expression in WT and *dy*$^{W-/-}$ fetal muscles; C2C12-WT and C2C12-KO cells cultured in flasks; and between rECM – in this case, each rECM combination was compared with another rECM combination separately. For example, WT x WT was compared with WT x KO, then with *dy*$^{W-/-}$ x WT, and then with *dy*$^{W-/-}$ x KO.

Student's t-test was also used to analyse proliferation differences between rECM by comparing the ratio of pH3 positive cells/total cell number in each rECM combination.

3

RESULTS

3.1 Characterization of decellularized matrices[1]

Decellularization is a process that aims at removing all cellular components, leaving only the extracellular matrix macro and microstructure intact. Our laboratory recently developed an effective decellularization protocol that ensures the preservation of laminin-α2 [45]. This protocol was established to create a 3D model for the study of LAMA2-CMD, focusing on the interactions between muscle cells and fetal extracellular matrix.

Throughout the protocol, the appearance of the isolated deep back muscle undergoes progressive changes (**Figure 3.1 A - D**). Initially, freshly isolated muscle masses appear reddish due to the presence of myoglobin. Following incubation in a hypotonic buffer, which lyses the cells and wash myoglobin, the tissue becomes white. As the tissue is treated with SDS, cell material is progressively removed, resulting in increasingly transparent samples. Finally, DNase treatment removes DNA, resulting in slightly smaller, transparent dECM.

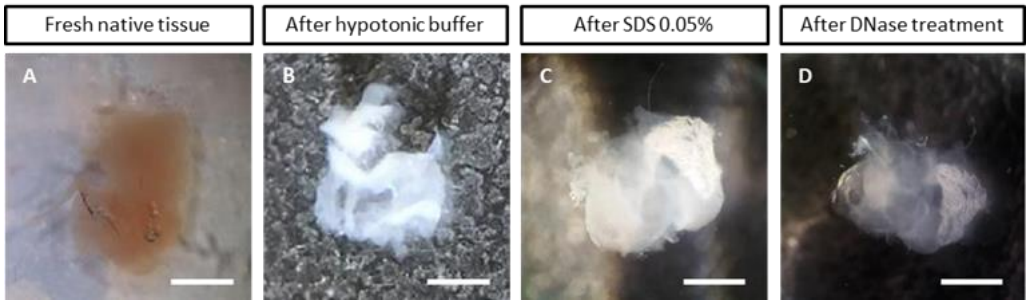

Figure 3.1 Morphology of the tissue throughout the decellularization process. Deep back muscle after isolation appears reddish due to the presence of myoglobin (A). As the decellularization protocol progresses and the cellular content is eliminated, the tissue becomes white (B) and ultimately transparent (C). After the final treatment with DNase, the sample became slightly smaller, resulting in a fully decellularized matrix (D). Scale bar = 1 mm.

[1] Some of the results described in this subchapter, including figure 3.1 and the original versions of figures 3.2 A and 3.3, were published in [45].

After decellularization the dECM generated by this protocol were characterized. A key aspect of decellularization is the complete removal of cellular components. To determine this, the amount of DNA was quantified in both NT and dECM from E18.5 fetal mouse skeletal muscle. This developmental stage was selected because it corresponds to the myogenesis phenotype that first manifests in LAMA2-CMD. The results showed a significant decrease, nearly 100%, in the amount of DNA after applying the decellularization protocol (**Figure 3.2 A**). To confirm the effectiveness of the process, we also used cytochemistry, in which dECM were labeled with methyl green to detect DNA and phalloidin to stain the actin cytoskeleton of the cells. As confocal microscopy uses three distinct channels to capture light of different wavelengths, the dECM were also immunostained for collagen IV, an extracellular matrix protein. The outcome clearly indicates that no phalloidin nor methyl green labeling is present, ensuring that the protocol was successful in eliminating every cellular component and DNA content (**Figure 3.2 B**). Moreover, collagen IV staining seems to be labeling the periphery of the myotubes previous location (**Figure 3.2 B** indicated by white arrow), showing that the matrix structure, in this case the BM, has been preserved, at least partially.

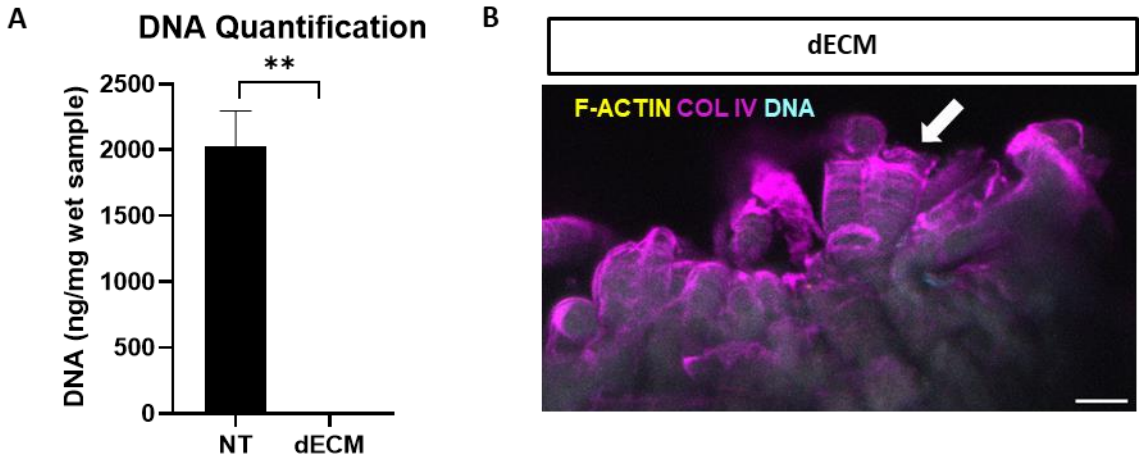

Figure 3.2 Characterization of decellularized matrices. (A) Comparison of DNA quantification in native tissue (NT) and decellularized extracellular matrix (dECM). The dECM shows a decrease in DNA content. N= 3 for both NT and dECM samples. Student's t-test showed a significant difference (**p<0.01). **(B)** Staining of dECM with methyl green (cyan), a DNA marker, phalloidin for F-actin filaments (yellow) and immunostaining for collagen type IV (magenta). The staining shows preservation of protein in the collagen fibers and a lack of cellular and DNA content. The white arrow represents the immunostaining of the periphery of the myotubes previous location. Scale bar: 20 μm. The decellularization protocol was effective in removing DNA and cells **(A, B).**

Another very important aspect of the decellularization process is the preservation of the ECM. To assess this, and after detecting the presence of collagen IV (**Figure 3.2 B**) we examined whether five key ECM proteins were retained after the decellularization protocol. This characterization was performed by western blot, both in NT and dECM (**Figure 3.3**).

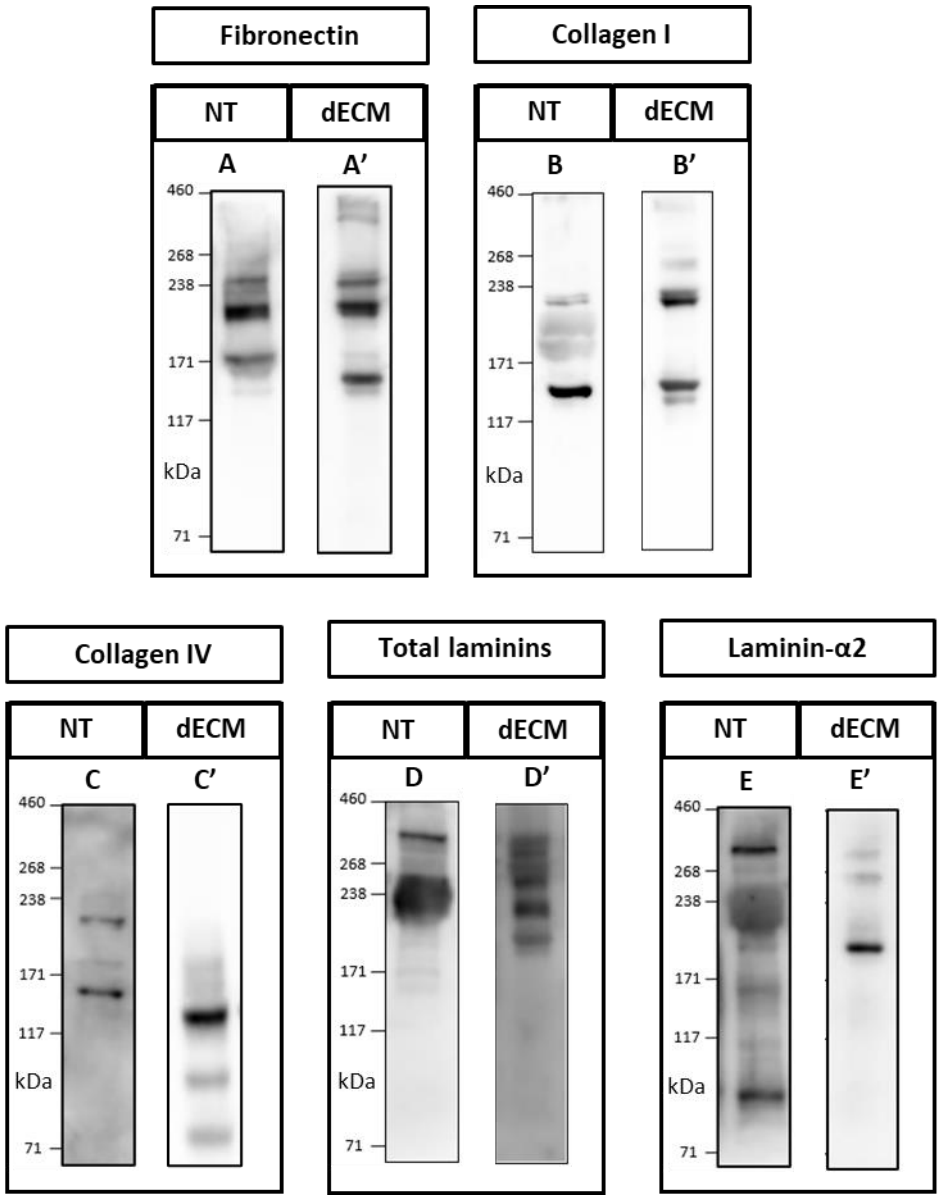

Figure 3.3 Characterization of the main ECM proteins in both native tissue and dECM. Western blot analysis was conducted to examine the interstitial matrix proteins in both NT samples **(A, B)** and dECM samples **(A', B')**, as well as the basement membrane proteins in NT **(C, D, E)** and dECM samples **(C', D', E')**. Even though some fragmentation and/or degradation of collagen I **(B'),** collagen IV **(C')**, total-laminins **(D')**, and laminin-α2 **(E')** occurred in dECM samples, the decellularization protocol effectively preserved the proteins.

Both IM and BM proteins were analyzed. The western blot results show that fibronectin (220 kDa) is not affected by the protocol, as the bands in both NT and dECM are identical (**Figure 3**

A, A'). However, for collagen I (120 kDa), instead of a single band, there are two smaller bands present in dECM, suggesting that this protein underwent some degree of degradation during the protocol (**Figure 3 B, B'**). Regarding the BM, analysis of collagen IV (160-190 kDa) showed that while three bands were detected in both NT and dECM, the bands in the dECM had a lower molecular weight, indicating some degradation (**Figure 3 C, C'**). For total-laminins (~200-400 kDa), using an antibody that detects all laminins, two bands were seen in NT with one of them being wide, while in the dECM, several fragmented bands appeared (**Figure 3 D, D'**). Concerning laminin-α2 (400 kDa) the results show that while in NT there are two bands present, in the dECM there are three bands of lower molecular weight (**Figure 3 E, E'**). These data suggest that although the proteins are present, some degradation or removal of proteins may have occurred during the decellularization protocol.

3.2 Expression levels of *Lama2* in three different models: *in vivo*, and 2D and 3D *in vitro*

Decellularized matrices can serve as a scaffold for cellular growth and proliferation. Recellularization of the dECM enables the study of cell-extracellular matrix interactions. Here, the combination of these two techniques was used to investigate these interactions during the onset of fetal stage LAMA2-CMD. WT and $dy^{W-/-}$ E18.5 deep back muscles were used to generate decellularized scaffolds. The C2C12 myoblast line (C2C12-WT) and a mutant line for the *Lama2* gene (C2C12-KO) were used as cells models. The C2C12-KO cells were generated previously by our host laboratory to be an *in vitro* tool to study LAMA2-CMD [41]. Given this, four different combinations were formed: WT dECM recellularized with C2C12-WT cells (WT x WT), and with C2C12-KO cells (WT x KO), and $dy^{W-/-}$ dECM recellularized with C2C12-WT cells ($dy^{W-/-}$ x WT) and with C2C12-KO cells ($dy^{W-/-}$ x KO) (**Figure 3.4**). These experimental conditions would allow to assess the cellular-extracellular niche interaction and examine how cells behave in terms of proliferation and differentiation when laminin-α2 is not present.

In addition to the 3D model, we also used *in vivo* native WT and $dy^{W-/-}$ deep back muscle at E18.5 and a 2D *in vitro* model where C2C12-WT and C2C12-KO cells were cultured in culture flasks. As a first approach, we characterized the expression levels of the *Lama2* gene in *in vivo* and *in vitro* 2D models by RT-qPCR (**Figure 3.5 A, A'**). As expected, the results showed a

significant decrease in *Lama2* levels in *dy*$^{W-/-}$ muscle and C2C12-KO cells compared to their WT counterparts, confirming the absence of laminin-α2 in these models and the success of the genetic manipulation in C2C12 cells. RT-qPCR was also performed using rECM. However, due to the difficulty of obtaining a high number of *dy*$^{W-/-}$ fetuses, the expression levels of *Lama2* could only be assessed in WT rECM (**Figure 3.5 A''**). In accordance to the 2D *in vitro* model, lower expression levels of *Lama2* were observed in C2C12-KO cells as compared to C2C12-WT (**Figure 3.5 A', A''**).

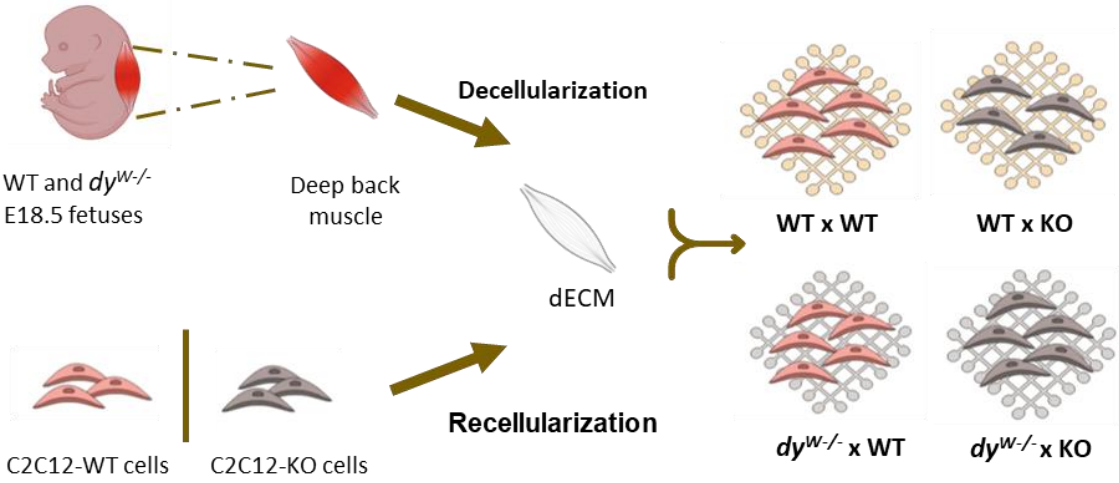

Figure 3.4 Schematic illustration of the decellularization and recellularization steps in the 3D *in vitro* model. Deep back muscles of WT and *dy*$^{W-/-}$ fetuses at E18.5 are decellularized and the generated dECM are then recellularized with C2C12-WT or C2C12-KO cells, forming four different combinations: WT dECM recellularized with C2C12-WT cells (WT x WT) and with C2C12-KO cells (WT X KO); *dy*$^{W-/-}$ dECM recellularized with C2C12-WT cells (*dy*$^{W-/-}$ x WT) and with C2C12-KO cells (*dy*$^{W-/-}$ x KO).

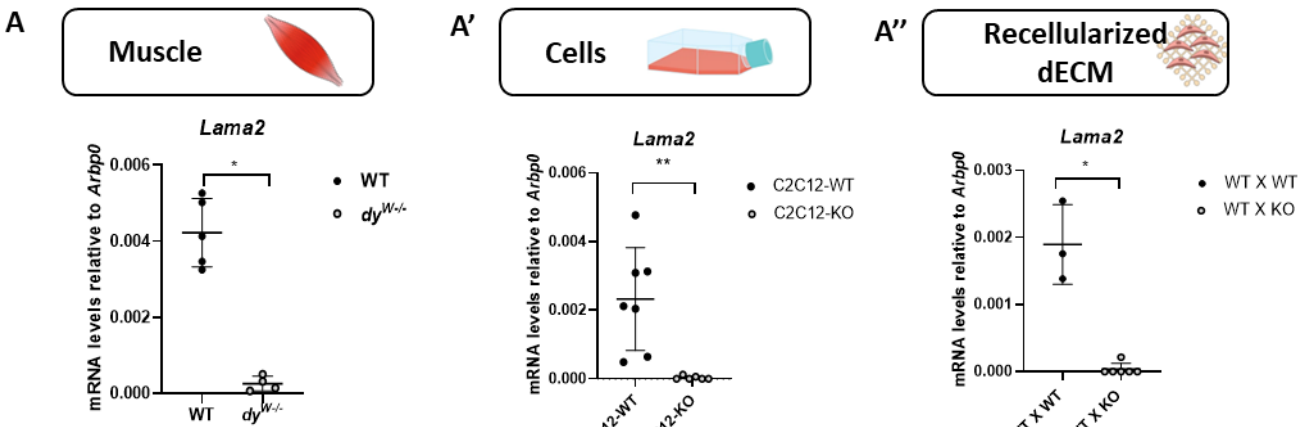

Figure 3.5 *Lama2* expression in *in vivo* and *in vitro* systems. Gene expression levels of *Lama2* in deep back muscles from WT and *dy*$^{W-/-}$ deep back muscles at E18.5 **(A)**, in C2C12-WT cells and C2C12-KO cells cultured in flasks **(A')**, and in WT rECM WT cultured for 8 days in growth medium **(A'')**, obtained by RT-qPCR. Transcription levels were normalized with the housekeeping gene *Arbp0*. Each dot represents an individual sample N=3-5 fetuses for each genotype. Statistical analysis was performed by using unpaired t-test, * $p<0.05$, ** $p<0.01$.

3.3 Impact of laminin-α2 absence on other ECM proteins

After verifying that *dy*$^{W-/-}$ muscles and C2C12-KO cells do not express *Lama2*, we investigated whether the absence of laminin-α2 affects the expression of other proteins found in the extracellular niche. This was evaluated by examining the expression of genes encoding proteins present in the BM and IM of the fetal muscle. RT-PCR analysis was performed on deep back muscle at E18.5, in cells cultured in flasks, and in rECM. Because rECM have a lower cell density than the other models, it was not always possible to analyze protein presence and content. For these matrices, immunohistochemistry was also used.

Previous studies have shown that both laminin-411 and laminin-511 could compensate for the absence of laminin-211 [48]. Thus, the expression level of the *Lama5* gene was evaluated. The results showed no significant differences in expression levels in either muscles or cells (**Figure 3.6 A, A'**). For immunohistochemistry, a pan-laminin antibody, which labels all laminins present in SM, was used. The results showed staining the previous location of myotube periphery (**Figure 3.6 B, C, D, E** indicated by yellow arrow) in all rECM, and in some areas, the staining suggest that intracellular laminins are present (**Figure 3.6 B - B'', C - C'', D - D'', E - E''** indicated by orange arrow). To determine if laminin-α2 was also expressed, an anti-laminin-α2 antibody was used. However, this antibody did not detect the protein in our hands under the present protocol.

In addition to laminin-211, collagen IV is a major component of the BM and these two proteins interact and create a network. Hence, the absence of laminin-211 may affect the expression levels of collagen IV. RT-qPCR results show a trend towards a higher expression of *Col4a1*, in WT muscles, but this difference is not statistically significant (**Figure 3.7 A**). However, the expression level of *Col4a1* is significantly higher in C2C12-WT cells compared to C2C12-KO cells (**Figure 7 A'**), indicating that the lack of laminin-211 may decrease the expression of collagen IV. The same pattern is observed in the rECM, although the difference is not significant (**Figure 3.7 A''**). Immunohistochemistry does not reveal any differences between the rECM but as for pan-laminins antibody, collagen IV labeling can be seen in the the periphery of the myotubes previous location (**Figure 3.7 B, C, D, E** indicated by yellow arrow) and in the cytoplasm of the C2C12-WT cells (orange arrow in **Figure 3.7 D**).

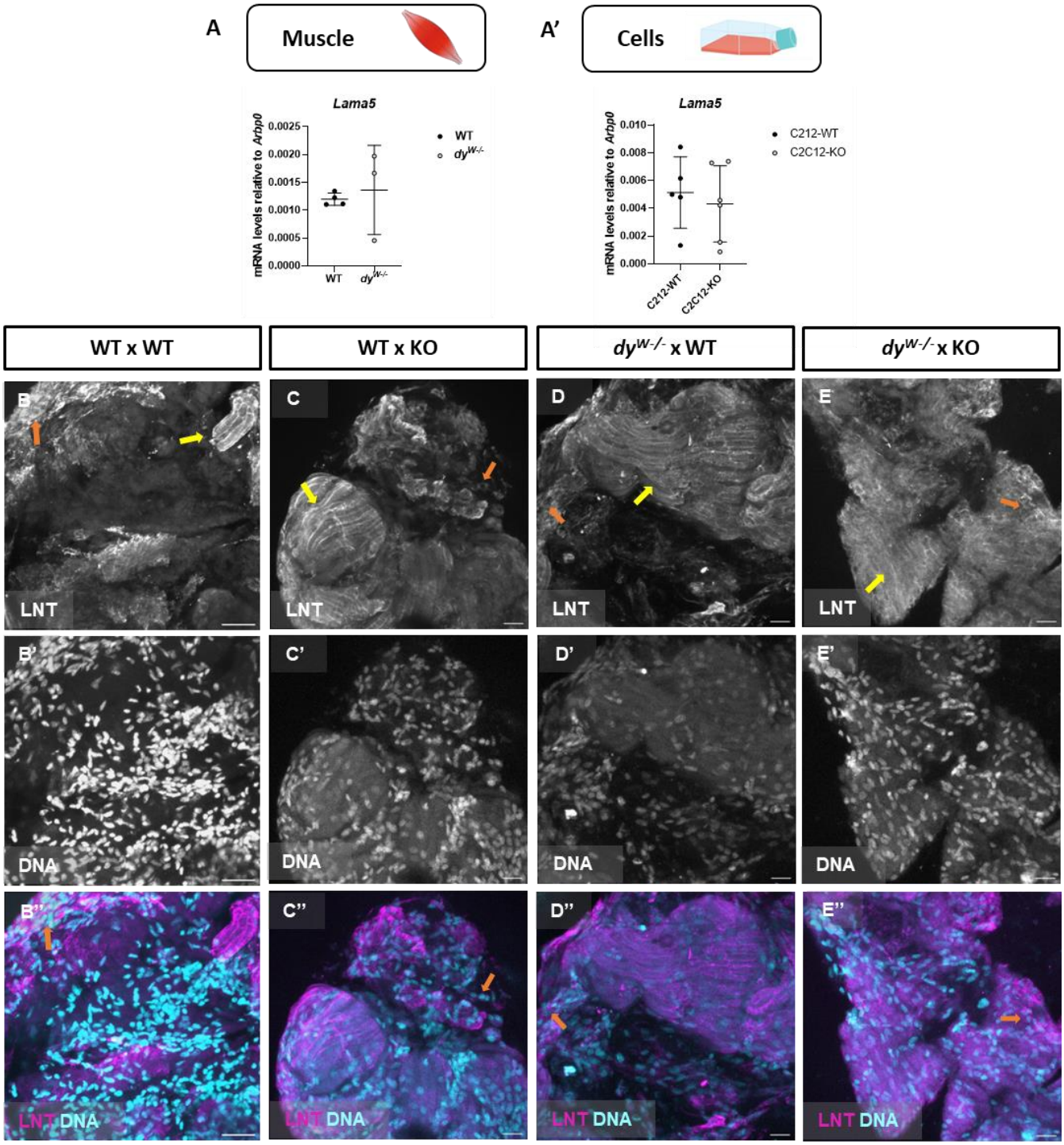

Figure 3.6 Characterization of laminins in *in vivo* and *in vitro* models. Gene expression levels of *Lama5* in deep back muscles from WT and $dy^{W-/-}$ E18.5 fetuses **(A)** and in C2C12-WT and C2C12-KO cells cultured in 2D **(A')**. Transcript levels were normalized with the housekeeping gene *Arbp0*. Each dot represents an individual sample N=3-4 fetuses for each genotype. Statistical analysis was performed using unpaired t-test. Immunohistochemistry in WT x WT **(B - B'')**, WT X KO **(C - C'')**, $dy^{W-/-}$ x WT **(D - D'')** and $dy^{W-/-}$ X KO **(E - E'')** for pan-laminin (LNT) **(B, C, D, E –** greyscale, and **B'',C'', D'', E'' -** magenta**)** and staining for DNA (methyl green) **(B', C', D', E' –** greyscale, and **B'',C'', D'', E'' –** cyan**)**. The color image **(B'', C'', D'', E'')** is a merge of the respective greyscale channels. Orange arrows represent laminins that are express by the cells. Yellow arrows represent the periphery of previous myotubes. Scale bar = 30 µm. The WT and $dy^{W-/-}$ rECM were cultured for 8 days in growth medium.

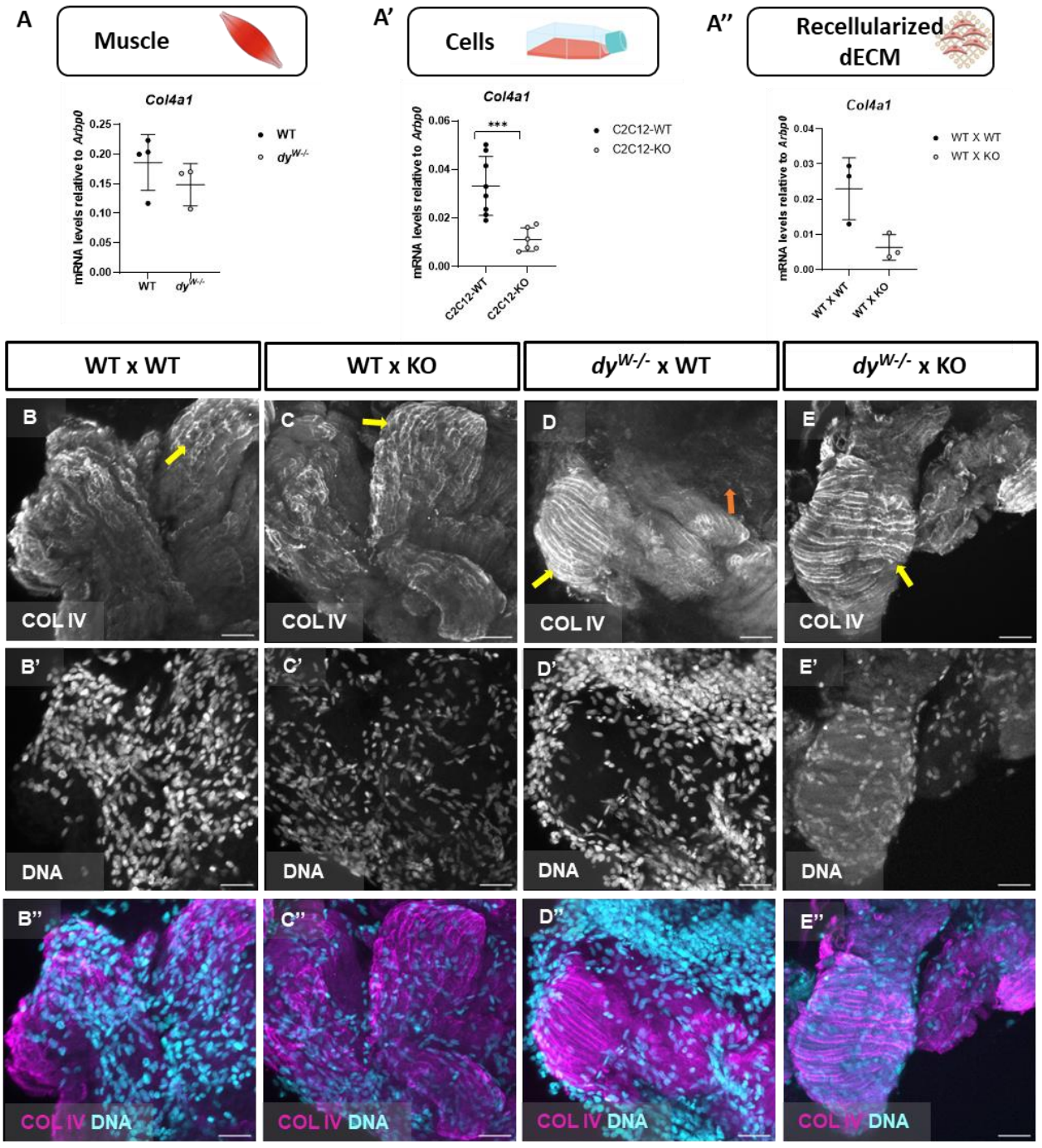

Figure 3.7 Characterization of collagen IV in *in vivo* and *in vitro* models. Gene expression levels of *Col4a1* in deep back muscles from WT and $dy^{W-/-}$ E.18.5 fetuses **(A)** , in cells cultured in flasks **(A')** and in recellularized WT and $dy^{W-/-}$ matrices cultured for 8 days in growth medium **(A'')**. Transcript levels were normalized with the housekeeping gene *Arbp0*. Each dot represents an individual sample N=3-4 fetuses for each genotype. Statistical analysis was performed using unpaired t-test. ***p<0.001. Immunohistochemistry in WT x WT **(B - B'')**, WT X KO **(C - C'')**, $dy^{W-/-}$ x WT **(D - D'')** and $dy^{W-/-}$ X KO **(E - E'')** for collagen IV **(B, C, D, E –** greyscale, and **B'', C'', D'', E''** – magenta**)** and staining for DNA (methyl green) **(B', C', D', E'** – greyscale, and **B'',C'', D'', E''** – cyan). The color image **(B'', C'', D'', E'')** is a merge of the respective greyscale channels. Orange arrows represent collagen IV that is express by the C2C12-WT **(D)**. Yellow arrows represent the periphery of previous myotubes. Scale bar = 30 µm. The WT and $dy^{W-/-}$ rECM were cultured for 8 days in growth medium.

Perlecan was also analyzed by the expression levels of the *Hspg2* gene. The results showed no significant differences in the amount of perlecan in either muscles or cells (**Figure 3.8 A**). However, there is a tendency for lower levels of *Hspg2* being expressed in $dy^{W-/-}$ and in C2C12-KO cells when compared with their WT counterparts (**Figure 3.8 A, A'**).

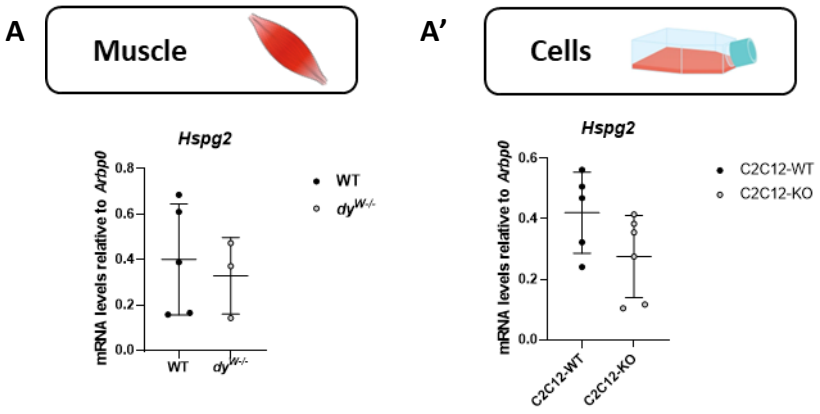

Figure 3.8 Characterization of perlecan *in vivo* and 2D *in vitro* model. Gene expression levels of *Hspg2* in deep back muscles from WT and $dy^{W-/-}$ E18.5 fetuses **(A)** and in cells cultured in flasks **(A')**. Transcript levels were normalized with the housekeeping gene *Arbp0*. Each dot represents an individual sample N= 3-5 fetuses for each genotype. Statistical analysis was performed using unpaired t-test.

In addition to BM Proteins, IM proteins were also analyzed. Fibronectin is a major protein found in the IM. The results showed no significant difference in either muscle or cells, indicating that the absence of laminin-α2 does not affect *fibronectin* gene expression (**Figure 3.9 A, A'**). Immunohistochemistry revealed that there are no differences between the rECM. However, it appears that C2C12-WT cells cultured in WT dECM exhibit slightly more fibronectin than C2C12-KO cells (orange arrow in **Figure 3.9 B**).

Collagen I is also present in the IM and, unlike collagen IV, it does not bind to laminin-211. Surprisingly, there is a tendency for higher *Col1a1* gene expression levels in $dy^{W-/-}$ individuals compared to WT individuals (**Figure 3.10 A**). However, in 2D *in vitro*, the expression levels of *Col1a1* show the inverse behavior, with a significantly higher expression of *Col1a1* in C2C12-WT cells than in C2C12-KO cells (**Figure 3.10 A'**). Unfortunately, due to the limited number of $dy^{W-/-}$ fetuses, it was not possible to draw conclusions about *Col1a1* expression levels in the rECM. Additionally, using immunohistochemistry we do not detect any difference in collagen I pattern between the rECM (**Figure 3.10 B**). It's worth mentioning that collagen I only appears

to be present in the ECM, with no indication of observable images suggestive of production by the cells in the 3D model.

These data suggest that laminin-α2 seems to interfere with BM proteins present in the contiguous BM (collagen IV and perlecan), but also with molecules that are present in the IM (collagen I).

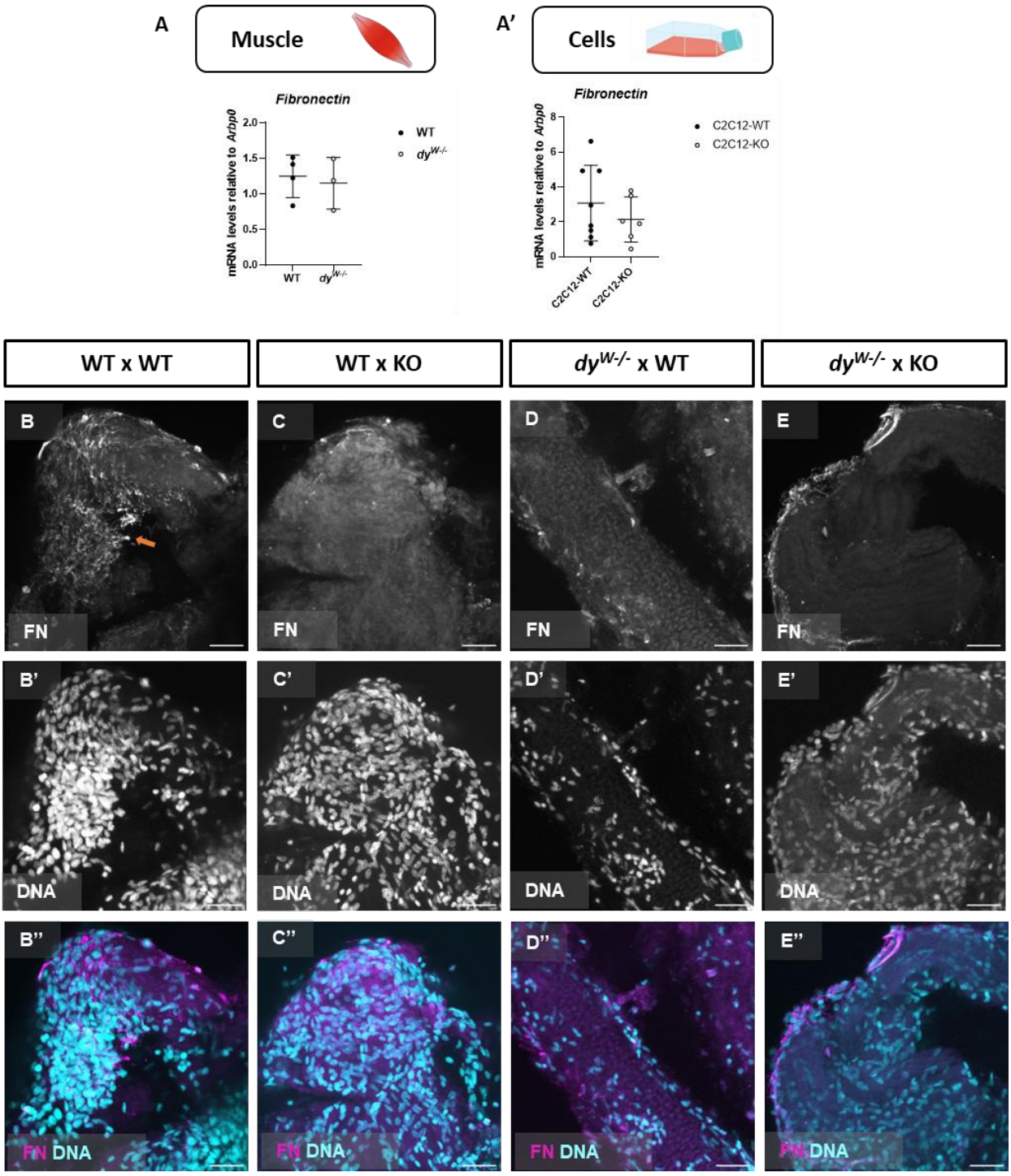

Figure 3.9 Characterization of fibronectin *in vivo* and *in vitro* models. Gene expression levels of *fibronectin* in deep back muscles from WT and $dy^{W-/-}$ E.18.5 fetuses **(A)** and in cells cultured in flaks **(A')**. Transcript levels were normalized with the housekeeping gene *Arbp0*. Each dot represents an individual sample N=3 fetuses for each genotype. Statistical analysis was performed by using unpaired t-test. Immunohistochemistry in WT x WT **(B - B'')**, WT X KO **(C - C'')**, $dy^{W-/-}$ x WT **(D - D'')** and $dy^{W-/-}$ X KO **(E - E'')** for fibronectin **(B, C, D, E** – greyscale, and **B'',C'', D'', E''** – magenta**)** and staining for DNA (methyl green) **(B', C', D', E'** – greyscale, and **B'',C'', D'', E''** – cyan**)**. The color image **(B'', C'', D'', E'')** is a merge of the respective greyscale channels. Orange arrows represent fibronectin that is express by the C2C12-WT **(B)**. Scale bar = 30 µm. The recellularized WT and $dy^{W-/-}$ matrices were cultured for 8 days in growth medium.

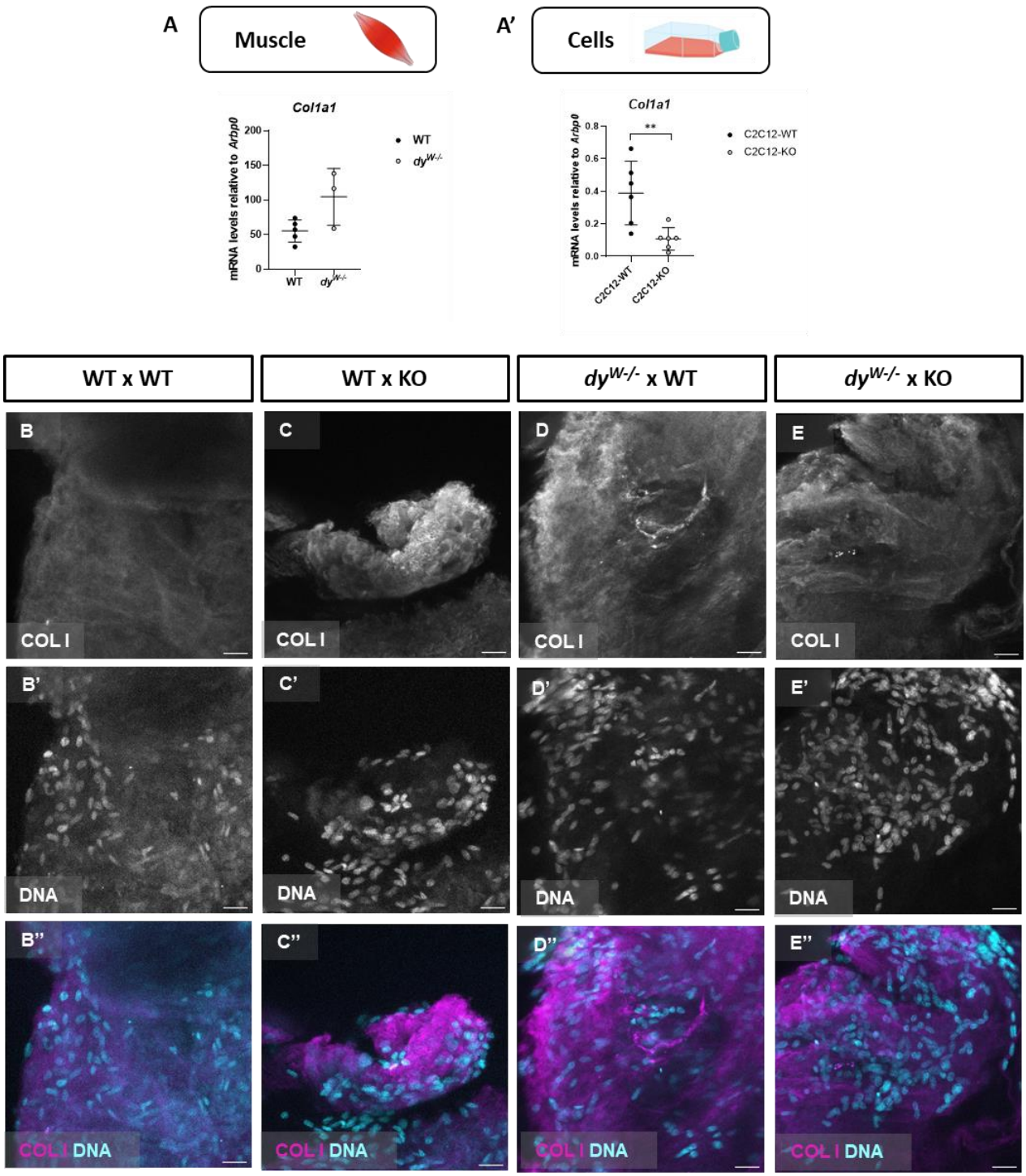

Figure 3.10 Characterization of collagen I in *in vivo* and *in vitro* models. Gene expression levels of *Col1a1* in deep back muscles from WT and *dy*$^{W-/-}$ E.18.5 fetuses **(A)** and in cells cultured in flaks **(A')**. Transcript levels were normalized with the housekeeping gene *Arbp0*. Each dot represents an individual sample N=3-5 fetuses for each genotype. Statistical analysis was performed by using unpaired t-test.** p<0.01. Immunohistochemistry in WT x WT **(B - B'')**, WT X KO **(C - C'')**, *dy*$^{W-/-}$ x WT **(D - D'')** and *dy*$^{W-/-}$ X KO **(E - E'')** for collagen I **(B, C, D, E** – greyscale, and **B'',C'', D'', E''** – magenta**)** and staining for DNA (methyl green) **(B', C', D', E'**– greyscale, and **B'', C'', D'', E''** – cyan**)**. The color image **(B'', C'', D'', E'')** is a merge of the respective greyscale channels. Scale bar= 30 µm. The recellularized WT and *dy*$^{W-/-}$ matrices were cultured for 8 days in growth medium.

3.4 Reduced expression of *Lama2* affects cell proliferation

After verifying that the absence of laminin-α2 leads to some perturbation in the extracellular niche, we asked whether its absence would also impact cell proliferation. Using RT-qPCR, the expression level of the *MKi67* gene, a proliferation marker, was evaluated in deep back muscle at E18.5, in 2D cells, and in rECM. The results showed no differences in muscle or in 2D grown cells (**Figure 3.11 A, A'**). However, in the rECM, a significant difference was observed after 8 days of culture: proliferation of C2C12-KO cells was much lower than C2C12-WT cells when cultured in WT dECM, indicating that the absence of laminin-211 in the cells negatively affects cell proliferation (**Figure 3.11 A''**). Unfortunately, only one $dy^{W-/-}$ individual was available for this experiment, therefore, although there is a trend for the cells to behave similarly in $dy^{W-/-}$ dECM, no clear conclusions can be drawn.

In a next step, we wanted to ascertain that the absence of laminin-211 impacts cell proliferation, and a resazurin assay was performed. This test is based on the fact that metabolically active cells reduce resazurin, a non-fluorescent blue dye, into resorufin, a highly fluorescent pink compound. Thus, the amount of resorufin is directly proportional to the number of viable cells and can be quantified by fluorescence measurement. The assay was conducted in two conditions: (1) cells cultured in dECM were allowed to proliferate for 12 days in growth medium, or (2) after 8 days of being cultivated in growth medium, the medium was changed to differentiation medium for 4 additional days.

The resazurin assay results show a significant difference between the WT X WT condition *versus* the $dy^{W-/-}$ x KO condition (**Figure 3.11 B**). In WT matrices, a significant difference in proliferation was also observed between the C2C12-WT and the C2C12-KO cells (**Figure 3.11 B**), which is also supported by the expression levels of the *MKi67* gene (**Figure 3.11 A''**). In $dy^{W-/-}$ matrices, neither C2C12-WT nor C2C12-KO cells exhibit any increase in proliferation over the course of eight days in culture (**Figure 3.11 B**). In the presence of a laminin-rich extracellular niche, C2C12-WT cells showed a significantly higher proliferation compared to $dy^{W-/-}$ matrices. The proliferation of C2C12-KO cells remains unaltered regardless of the matrix. Thus, over an 8-day period, a higher proliferation can be seen in WT X WT, while the other rECM (WT x KO, $dy^{W-/-}$ *x* WT and $dy^{W-/-}$ x KO) do not exhibit an increase in the number of cells.

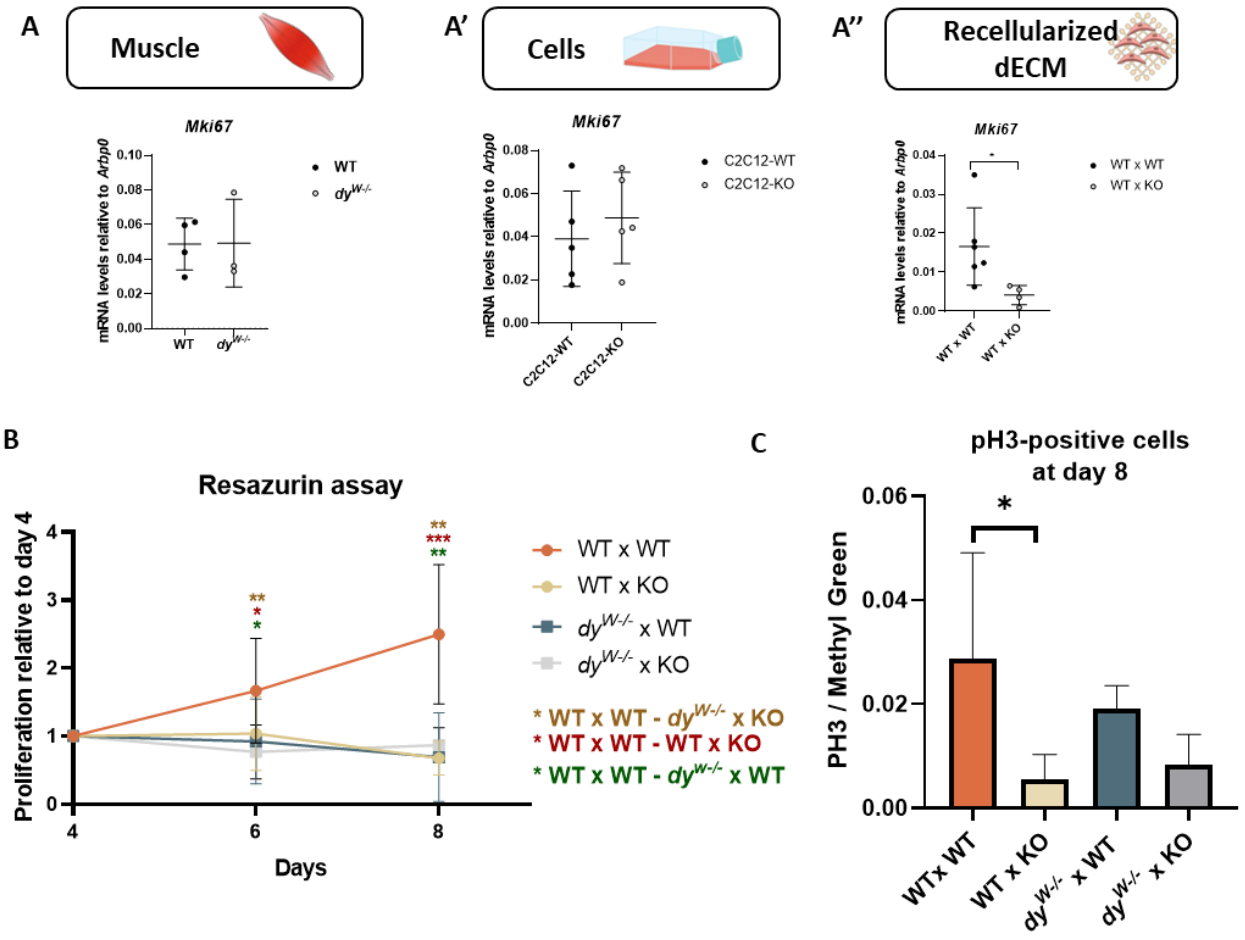

Figure 3.11 Absence of laminin-α2 affects proliferation. Gene expression levels of *MKi67* (proliferation marker) in WT and $dy^{W-/-}$ deep back muscles at E18.5 **(A)**, in WT-C2C12 cells and KO-C2C12 cells cultured in flasks **(A')**, and in recellularized WT and $dy^{W-/-}$ matrices cultured for 8 days in growth medium **(A'')**, obtained by RT-qPCR. Transcription levels were normalized with the housekeeping gene *Arbp0*. Each dot represents an individual sample N=4-7 fetuses for each genotype. Statistical analysis was performed by using unpaired t-test, * $p<0.05$. **(B)** Cell proliferation was monitored in WT and $dy^{W-/-}$ rECMs on day 4, 6 and 8 using a resazurin test. Data was plotted relative to day 4 to analyze proliferation. N (WT) = 16, N ($dy^{W-/-}$) = 8 independent experiments done with 3 technical replicates each. Statistical analysis was performed with student t-test. P-value: * $p<0.05$; ** $p<0.01$; *** $p<0.001$. **(C)** Graph showing the ratio of phospho-Histone 3 (pH3) positive cells in rECM. The rECM were immunostaining for pH3 and counterstained with methyl green (DNA marker). The ratio was obtained by dividing the number of pH3-positive cells immunostained by the total number of cells stained with methyl green. Graph shows the data from various independent experiments, N (WT rECM) = 5, N ($dy^{W-/-}$)= 3. Statistical analysis was performed with student t-test. P-value: * $p<0.05$; ** $p<0.01$.

In addition to RT-qPCR and the resazurin assay, an additional quantitative analysis was performed using the recellularized matrices. Phospho-Histone 3, a marker for late G2/M phase (cells undergoing mitosis), immunohistochemistry was performed on day 8. The rECM were

immunostaining for pH3 and counterstained with methyl green, in order to detect the total number of cells (**Figure 3.11 C**).

In WT rECM, the number of pH3-positive cells was significantly higher for C2C12-WT cells than for C2C12-KO cells (**Figure 3.11 C**), consistent with the RT-qPCR and resazurin assay results (**Figure 3.9 A'', B**). Although no significant differences were observed in the other rECM, the trend was similar to that of the resazurin assay, with C2C12-WT cells showing more pH3-positive cells in WT rECM than in $dy^{W-/-}$ rECM (**Figure 3.11 C**). The number of pH3-positive cells in C2C12-KO cells remained low irrespective of the dECM type.

Altogether, these results indicate that the absence of laminin-α2 in the extracellular environment impairs the proliferation of C2C12-WT cells. On the other hand, the presence of laminin-α2 in the extracellular environment is not sufficient to improve the proliferation of C2C12-KO cells. This suggests that the presence of functional laminin-α2 in the cells is essential for normal cell proliferation. Both the cellular and extracellular components must contain functional laminin-α2 for proper cell proliferation to occur.

Since the absence of laminin-α2 may also affect differentiation, we also investigated whether changing the culture conditions where the cells were growing from growth medium to differentiation medium had an impact on cell proliferation. For this purpose, we measured the proliferation at day 12 by dividing the fluorescent levels of resazurin measurements by the levels at day 8, which is the time point from which the cells in rECM were incubated with differentiation medium. Interestingly, while different culture media had no effect on cell activity in $dy^{W-/-}$ rECM, differentiation media led to a higher cell proliferation in WT rECM, especially for C2C12-KO cells (**Figure 3.12 A**).

To determine if indeed cells grown in WT rECM incubated in differentiation medium proliferated more, the number of pH3-positive cells was quantified **(Figure 3.12 B**). Surprisingly, the results showed the opposite effect. When grown in WT matrices, C2C12-WT cells show a higher number of pH3-positive cells when incubated in growth medium than in differentiation medium (**Figure 3.12 B**). However, different culture media do not have any significant impact on WT matrices grown-C2C12-KO cell proliferation (**Figure 3.12 B**), apparently contradicting the previous results (**Figure 3.12 A**). C2C12-KO cells proliferate significantly less than C2C12-WT when cultured in differentiation medium in WT matrices for 12 days (p-value < 0.01 in **Figure**

3.12 B). In *dy*$^{W-/-}$ rECM, we observed no differences in the number of pH3-positive cells, regardless of the culture medium or the type of cells.

Overall, this data supports our previous findings, indicating that laminin-α2 has an impact in cell proliferation and that this effect persists regardless of whether or not the cells are induced to differentiate.

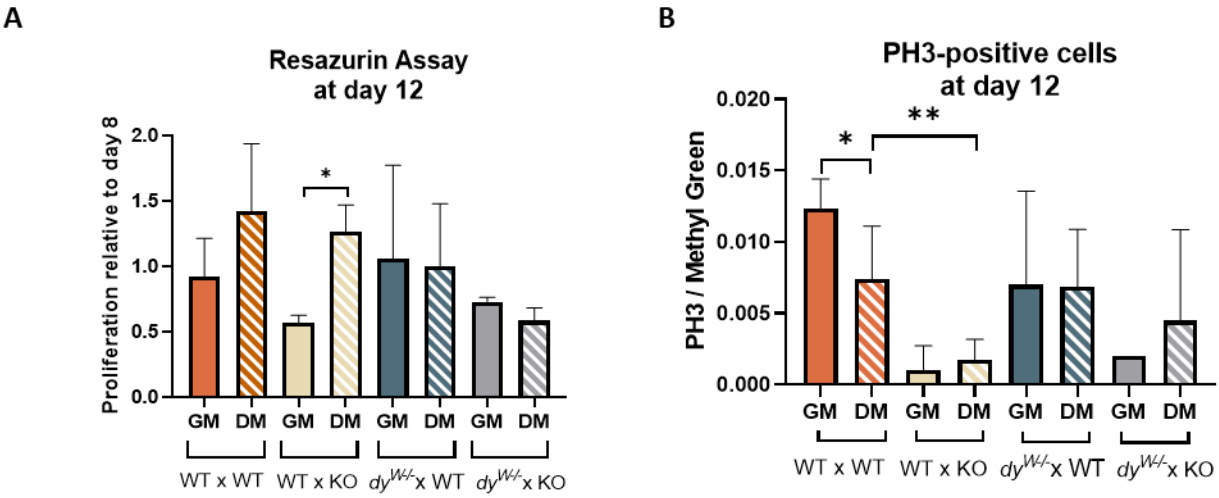

Figure 3.12 Effect of different culture media in cell proliferation in recellularized matrices. (A) WT and *dy*$^{W-/-}$ rECM were cultured under two different experimental conditions: 12 days in a normal growth medium, or 8 days in a growth medium (GM) followed by 4 days in differentiation medium (DM). Cellular proliferation was monitored on days 8 and 12 under both conditions using the resazurin assay. To compare the effect of different culture media, the cell viability on day 12 was analysed and the data was plotted relative to day 8, the day from which the matrices were incubated with differentiation medium. For both medium: N (WT rECM) = 5; N (*dy*$^{W-/-}$ rECM) = 3. Statistical analysis was performed with student t-test. P-value:* $p<0.05$. **(B)** Graph showing the ratio of phospho-histone 3 (pH3) positive cells in rECM. The rECM were immunostained for pH3 and counterstained with methyl green. The graph shows the data from various independent experiments. Growth medium: N (WT x WT) = 5; N (WT x KO) = 3, N (*dy*$^{W-/-}$ x WT) = 3 , N (*dy*$^{W-/-}$ x KO) = 2. Differentiation medium: N (WT x WT) = 8; N (WT x KO) = 6, N (*dy*$^{W-/-}$ x wt) = 3, N (*dy*$^{W-/-}$ x KO) = 2. Statistical analysis was performed with student t-test. P- value: * $p<0.05$; ** $p<0.01$.

3.5 Reduced expression of *Lama2* affects cells differentiation

The previous findings indicate that the absence of laminin-211 results in impaired cell proliferation. In a further step, we wanted to assess whether the differentiation process was also impacted. Previous studies in our research group lead to the finding of a deficiency in the number of myogenin-positive cells in $dy^{W-/-}$ individuals at E18.5 [22]. Hence, the expression levels of the *MyoG* gene, which encodes for myogenin, were analyzed using RT-qPCR. This analysis was performed in deep back muscles at E18.5, in C2C12-WT and C2C12-KO cells, and also in WT rECM.

RT-qPCR results did not reveal differences in *MyoG* expression in WT and $dy^{W-/-}$ muscles, even though we could detect a slight increase *MyoG* expression in $dy^{W-/-}$ muscles (**Figure 3.13 A**). A significant difference was observed in cells, with C2C12-WT cells expressing more *MyoG* than C2C12-KO cells when cultured in 2D (**Figure 3.13 A'**). Surprisingly, when these cells were cultured for 8 days in dECM with functional laminin-α2, a significant higher expression of *MyoG* was observed in C2C12-KO cells when compared with C2C12-WT cells **(Figure 3.13 A'')**.
In fact, histochemical staining with phalloidin, a fluorescent toxin that labels the actin cytoskeleton of cells, suggests that C2C12-KO cells cultured in a 3D substrate for 8 days display a tendency to align more than C2C12-WT cells. This trend occurs in both WT and $dy^{W-/-}$ matrices-grown cells (indicated by the magenta arrows in **Figure 3.13 C'', E''**). Indeed, C2C12-WT cells appear to be more homogeneously distributed throughout the matrices and to align poorly (**Figure 3.13 B, D**).

Results from myosin heavy chain (a later marker of differentiation) labeling revealed that, irrespective of the alignment of C2C12-KO cells in rECM, no evidence of differentiation was seen in these cells, nor in any other experimental situation, as myosin heavy chain was not detected in any of the rECM after 12 days in culture. In a subsequent experiment, differentiation was induced: after 8 days growing in culture with growth medium, the rECM were further grown for 4 days in differentiation medium. As a result, multinucleated and well-defined myotubes were observed in the WT x WT (**Figure 3.14 A', A'''** indicated by the dashed orange line and arrow). In some cases, these cells form a multinucleated spherical myosin-positive structures (**Figure 3.14 A', A'''** indicated by the dashed blue lines and arrows). Although these structures are more frequent in the WT x WT they also occur in the $dy^{W-/-}$ x WT. On the other hand, even though C2C12-KO cells display the alignment behavior previously described, (indicated by

white arrows in **Figure 3.14 B''', D'''**), they never manage to form myotubes or spherical multi-nucleated structures, even when grown in differentiation medium in both types of dECM (**Figure 3.14 B', D'**).

It was hypothesized that the differentiation of C2C12-KO cells could require additional time, so the culture period maintaining cells growing in differentiation medium was extended to 3 additional days. As a result, C2C12-WT cells formed myotubes and multinucleated spherical structures, as expected. However, no myosin heavy chain was ever detected in C2C12-KO cells for this experimental period. Therefore, these results indicate that the lack of laminin-α2 in the cells seems to give rise to problems in differentiation, as they are not able to form myotubes. Although myotube formation occurs in the *dy*$^{W-/-}$ grown WT cells, it is less frequent, suggesting that the absence of laminin-α2 in the substrate also impacts differentiation.

Overall, these data suggest that C2C12-KO behave as cells trying to initiate the differentiation program (less proliferation, more alignment, higher *MyoG* expression) but somehow fail to fully differentiate (inability to express myosin and form elongated myotubes).

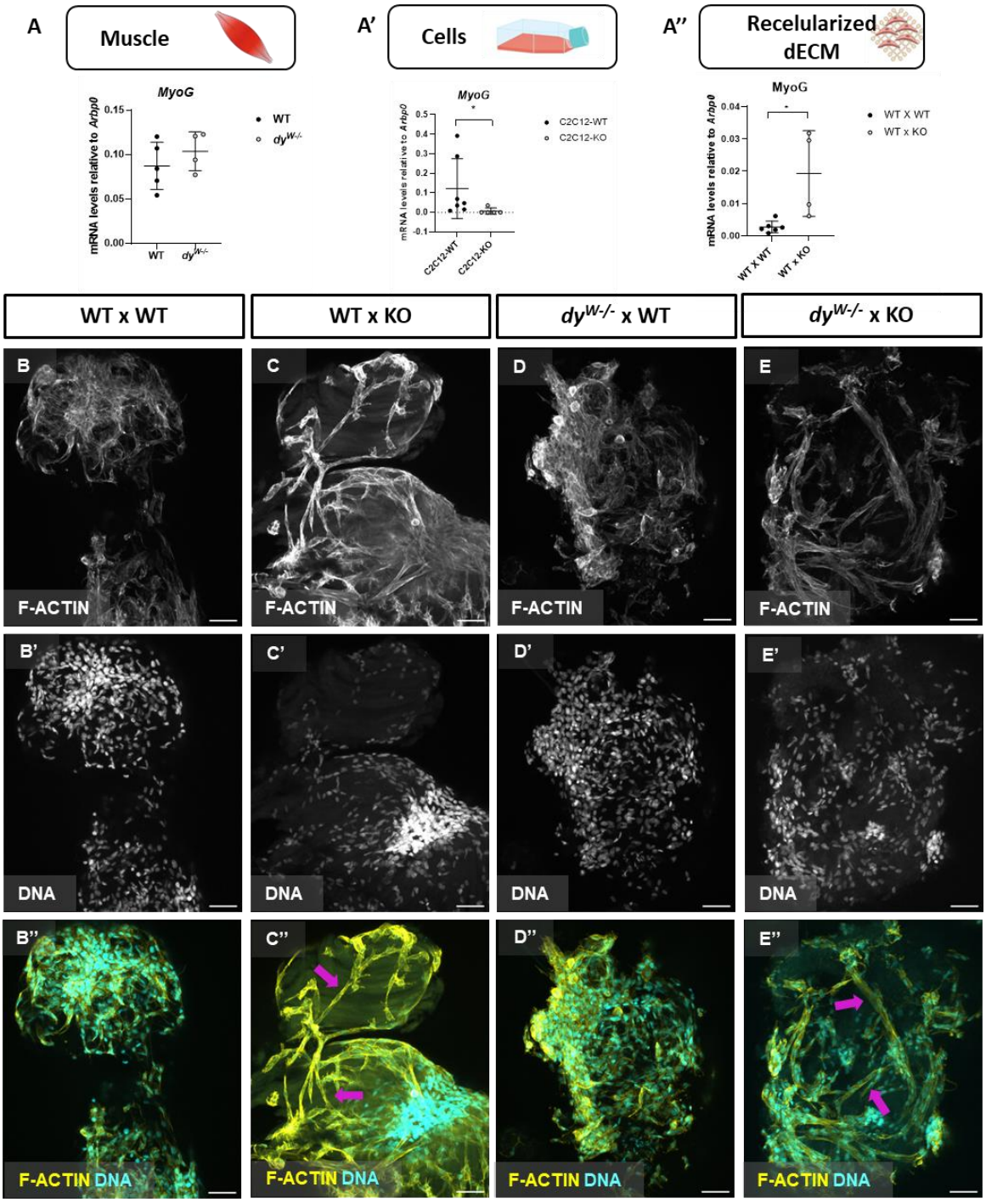

Figure 3.13 C2C12-KO cells C2C12-KO cells begin to express more *MyoG* and are more aligned, compared to their WT counterpart. Gene expression levels of *MyoG*, a differentiation marker, in deep back muscles from WT and *dy*$^{W-/-}$ E.18.5 fetuses **(A)**, in cell cultured in flasks **(A')** and in WT rECM cultured for 8 days in growth medium **(A'')**. Each dot represents an individual sample n=3-4 fetuses for each genotype. Statistical analysis was performed by using unpaired t-test, * $p<0.05$. Cytochemistry staining in WT x WT **(B - B'')**, WT X KO **(C - C'')**, *dy*$^{W-/-}$ x WT **(D - D'')** and *dy*$^{W-/-}$ X KO **(E - E'')** for f-actin (phalloidin) **(B, C, D, E** – greyscale, and **B'',C'', D'', E''** – yellow**)** and for DNA (methyl green**) (B', C', D', E'** – greyscale, and **B'',C'', D'', E''** – cyan**)**. The color image **(B'', C'', D'', E'')** is a merge of the respective greyscale channels. Pink arrows represent aligned cells **(C', E')**. Scale bar = 60 µm. WT and *dy*$^{W-/-}$ rECM were cultured for 8 days in growth medium.

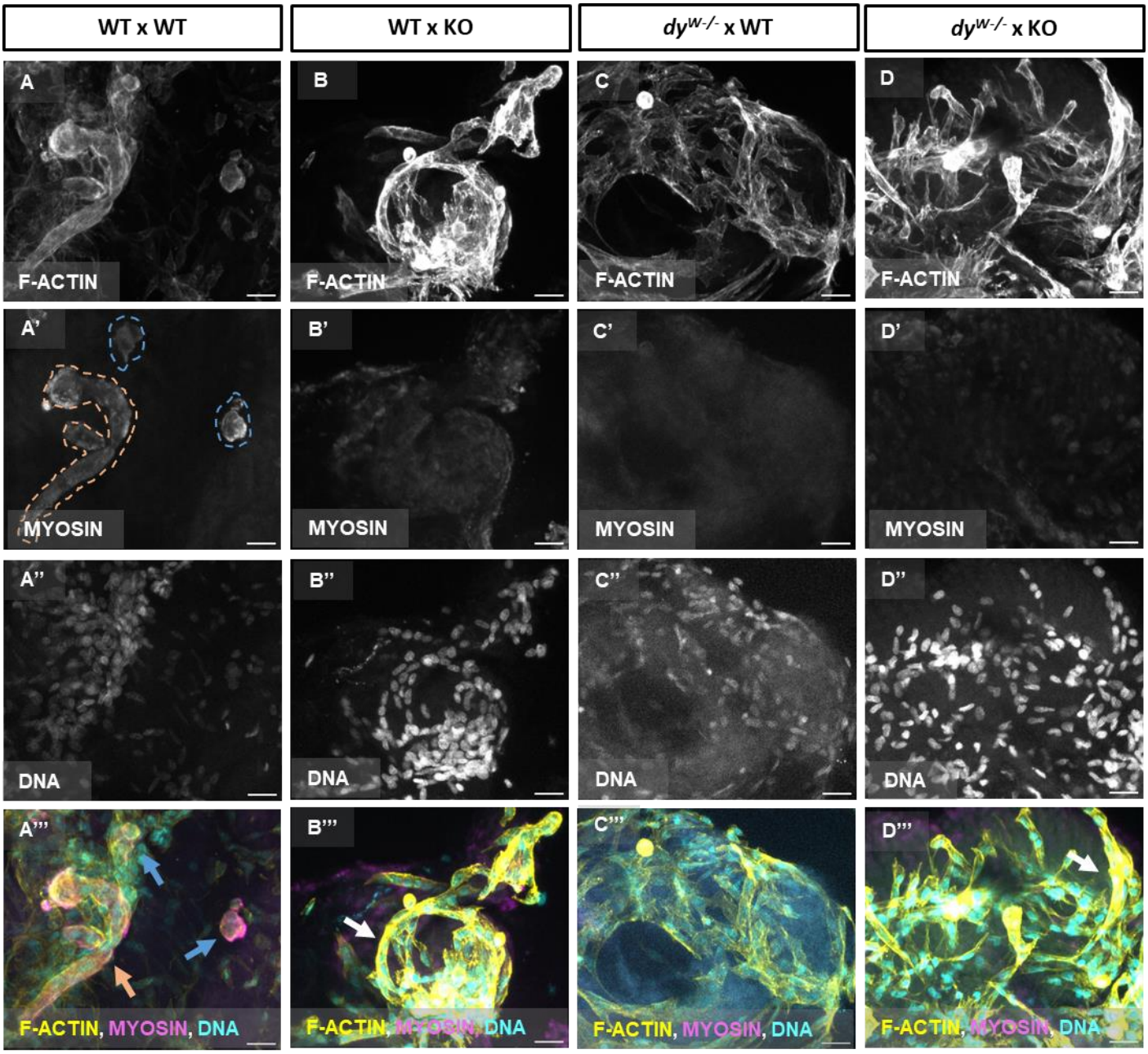

Figure 3.14 Although C2C12-KO organize as aligned cells only C2C12-WT in WT rECM form elongated multinucleated myotubes. Standing for f-actin (phalloidin) **(A, B, C, D** - greyscale and **A''', B''', C''', D'''** - yellow**)**, myosin heavy chain **(A', B', C', D'** - greyscale and **A''', B''', C''', D'''** - magenta**)** and DNA (methyl green) **(A'', B'', C'', D''** -greyscale and **A''', B''', C''', D'''** - cyan**)** in WT X WT **(A – A''')**, WT X KO **(B – B´´´)**, *dy*$^{W-/-}$ X WT **(C – C''')** and *dy*$^{W-/-}$ X KO **(D – D''')**. WT and *dy*$^{W-/-}$ matrices were cultured for 8 days in growth medium followed by 4 days in differentiation medium. Scale bar = 30 µm. Orange arrow **(A''')** and dashed lines **(A')** represent an elongated multinucleated myotube. Blue arrows **(A''')** and dashed lines represents spheric multinucleated structures **(A')**. White arrow represents aligned C2C12- KO cells **(B''', D''')**.

4

DISCUSSION

LAMA2-CMD results from genetic mutations in the *LAMA2* gene, which encodes for the α2 subunit, present in laminin-211 and laminin-221. Recent studies conducted by our research group, using the *dy*$^{W-/-}$ mouse as a model, have revealed that LAMA2-CMD begins to develop *in utero*, specifically during secondary myogenesis between embryonic days E17.5 and E18.5. During this phase a reduction in the number of MuSCs as well as a reduction in the size of muscle fibers can be observed, although the mechanisms that trigger these effects are not yet well understood. Thus, there is a need for a better understanding of the cellular and molecular processes that occur during the development of this disease.

The primary goal of this thesis was not only to examine how the absence of laminin-α2 affected the other proteins in the extracellular matrix, but also to understand how the absence of laminin-α2 impacted the interactions between cells and their extracellular environment in the onset of LAMA2-CMD, namely during the fetal developmental stage of the disease.

Silva *et al.* developed a decellularization protocol for mouse fetal heart that showcased the ability of dECMs to promote and preserve key features of the cardiac ECM, thereby facilitating the growth of fetal cardiomyocytes [49]. Recently, our research group adapted this 3D *in vitro* model for decellularized fetal skeletal muscle, and subsequently recellularized with muscle cells [45]. The decellularization process removes almost all the cellular components, including DNA residues (as shown in the **Figure 3.2**), while preserving the main proteins of the extracellular matrix (**Figure 3.3**). Some degree off degradation/fragmentation of collagens and laminins in dECM matrices was observed, as show by western blot results, **Figure 3.3 B', C', D', E'**), most

probably due to the decellularization protocol, namely the SDS incubation step that disrupts the proteins ultrastructure [43][45]. The subsequent adhesion, proliferation, and *de novo* synthesis of proteins by cells cultured in these matrices (as shown in the **Figures 3.6 B-E; Figure 3.7 D and Figure 3.9 B**) demonstrate that this model can closely mimic *in vivo* conditions. Therefore, rECM allows for the study of the interactions between the cells, their cellular niche and the general extracellular environment.

Using this 3D model, four different rECM were generated (WT x WT; WT x KO, $dy^{W-/-}$ x WT and $dy^{W-/-}$ x KO) to establish a platform with which we could investigate the influence of laminin-α2 on cellular-extracellular interactions. To mimic as closely as possible what occurs *in vivo*, the most suitable cell type to use would be MuSC from WT and $dy^{W-/-}$ mice. However, due to the challenging protocol for their collection and maintenance in culture, we used the C2C12 cell line, and the C2C12-KO cell line that was stablished by our host laboratory to be used as an *in vitro* tool to study LAMA2-CMD. The *in vivo* model of E18.5 WT and $dy^{W-/-}$ fetal muscle was also used, as well as 2D *in vitro* culture of C2C12-WT and C2C12-KO cells.

The absence of *Lama2* gene expression in $dy^{W-/-}$, C2C12-KO cells, and rECM (**Figure 3.5 A - A''**) suggests that these models can effectively be used to evaluate the effects of laminin-α2 deficiency in LAMA2-CMD.

4.1 Absence of laminin-α2 affects other ECM proteins

Laminin-211 plays a crucial role as a major component of the BM and is involved in the early stages of SM development. Its interactions with several molecules and receptors make it critical for maintaining the integrity of the extracellular environment. Consequently, the absence of laminin-α2 can disrupt other proteins present in the extracellular environment, leading to a range of side effects. Proteomic and transcriptomic studies have revealed that LAMA2-CMD affects the expression of multiple proteins, particularly those involved in metabolic processes, extracellular matrix homeostasis, and some proteins associated with inflammation and fibrosis [50]–[52].

Lower levels of *Col4a1* expression are observed in $dy^{W-/-}$ muscle, in C2C12-KO cells, and in C2C12-KO cells cultured on WT matrices (**Figure 3.7 A - A''**). Collagen IV, as well as laminin-

211, is a major constituent of the BM. These two molecules bind to each other and form a well-defined network that helps to stabilize the BM. Therefore, it was expected that the absence of laminin-α2 would affect the expression of this protein. Regrettably, an insufficient number of $dy^{W-/-}$ fetuses hampered the possibility of generating enough $dy^{W-/-}$ rECM for the study of *Col4a1* expression. Futhermore, immunohistochemistry for collagen IV did not reveal any observable differences between the rECM. Lower levels of *Hspg2*, which encodes for perlecan, are also observed in $dy^{W-/-}$ individuals and in C2C12-KO cells, although not significantly (**Figure 3.8 A, A'**). This proteoglycan present in the BM is responsible for stabilizing the collagen IV network and reinforcing the laminin network through its interaction with nidogen. Therefore, it seems that the absence of laminin-211 leads to a reduction of collagen IV and perlecan, which may destabilize the BM. Unfortunately, due to technical difficulties, it was not possible to analyse the *Hspg2* gene expression on the rECM, nor was it possible to stain perlecan by immunohistochemistry.

Col1a1 seems to be more expressed in $dy^{W-/-}$ fetuses, but in the 2D *in vitro* model, C2C12-KO cells show lower levels of *Col1a1* expression (**Figure 3.10 A, A'**). Although myoblasts and C2C12 cells are capable of synthesizing collagen I, this molecule is predominantly produced by fibroblasts [53], [54]. Therefore, the increased expression levels of *Col1a1* in $dy^{W-/-}$ individuals may be due to the action of fibroblasts rather than myoblasts. Higher levels of collagen I expression are often associated with fibrotic events [53] and fibrosis, along with inflammation, is one of the hallmarks of LAMA2-CMD [30], [55]. In fact, several studies show that higher values of this protein are detected in model mice for LAMA2-CMD [26], [53], [55], [56]. However, while this increase typically occurs after birth [55], our data suggest that this fibrosis process may start during fetal development. Fibronectin is another protein associated with fibrosis [54], and as for collagen I, higher levels of fibronectin are observed postnatally in patients and model mice for LAMA2-CMD [55]–[57]. However, our results show no differences between WT and $dy^{W-/-}$ muscle, nor between C2C12-WT and C2C12-KO cells in 2D (**Figure 3.9 A, A'**).

Both fibronectin and collagen I are regulated by TGF-β, which is one of the main culprits responsible for the fibrotic response in muscle disorders [56] and TGF-β has been shown to be overactivated in animal models for LAMA2-CMD [55], [56]. This activation of TGF-β consequently leads to an increased expression of genes that code for ECM proteins such as fibronectin, collagen I, and periostin [55]. Although our results show that fibronectin is not affected, we hypothesize that the trend for higher levels of *Col1a1* in $dy^{W-/-}$ muscle (**Figure 3.10 A**) can

suggest that the fibrosis process, which is characteristic of LAMA2-CMD patients, could begin to develop *in utero*.

The ECM is a highly dynamic system that plays a crucial role in maintaining SM homeostasis. In the absence of laminin-211, alternative mechanisms can be activated to compensate for its absence. It has been suggested that other forms of laminins, such as laminin-511 and laminin-411, may compensate for the lack of laminin-211 [58]. However, Nunes *et al.* observed no compensatory effects of these two proteins. Similarly, our results show no difference in the expression levels of the *Lama5* gene (**Figure 3.6 A, A'**). Additionally, immunohistochemistry for total laminins in the rECM did not reveal any observable differences (**Figure 3.6 B - E**). While it is not possible to determine which specific laminins are being expressed, it is clear that both C2C12-WT and C2C12-KO cells have the capacity to produce laminins regardless of the presence or absence of laminin-211 in the matrices (orange arrows in **Figure 3.6 B-E**).

Overall, the results suggest that the absence of laminin-α2 may have significant effects on the expression of other proteins in the ECM, particularly collagen IV. While our study did not assess the expression of the main laminin receptors, previous studies in LAMA2-CMD patients and mouse models have indicated a reduction in the integrin receptor in response to the lack of laminin-211 [59], [60]. In addition, the absence of laminin-α2 may also contribute to the overexpression of proteins involved in the fibrosis process, such as collagen I and fibronectin [52], [53], [55]. Our data regarding collagen I expression may further suggest that these fibrotic processes could initiate during fetal development. However, further studies are needed to elucidate the underlying mechanisms and to identify potential treatments to improve these processes.

4.2 Laminin-α2 is important for cell proliferation

While laminin-111 plays a role in myoblast proliferation, the expression of laminin-211 is associated with the process of myotube fusion and stability [61]. Consequently, few studies have investigated the importance of laminin-211 in proliferation [62]. Our results from the expression of *MKi67*, a proliferation marker, indicate no differences *in vivo* or *in vitro* for 2D cells (**Figure 3.11 A, A'**). However, in WT rECM, a lower expression level of this marker is observed in

C2C12-KO cells, suggesting that the absence of laminin-α2 may affect proliferation in cells growing in dECM (**Figure 3.11 A''**).

The concept that cell proliferation may be compromised in individuals with LAMA2-CMD is supported by the reduced detection of pH3 and lower proliferation shown over a 12-day period in the $dy^{W-/-}$ x KO situation (**Figure 3.11 B, C**). Proliferation defects are also noticeable in WT x KO and $dy^{W-/-}$ x WT, where either the extracellular environment or the cells lack functional laminin-211 (**Figure 3.11 B, C)**. This suggests that the presence of functional laminin-211 in one of the components (cells or ECM) is not sufficient to reverse the general effects of laminin-α2 absence in cell proliferation.

Several experiments have shown that myoblast proliferate more when cultured on laminin-coated substrates [63], [64]. This fact supports the observation that C2C12-WT cells proliferate more in a WT matrix compared to matrices devoid of laminin-211 ($dy^{W-/-}$ matrix) (**Figure 3.11 B**).

Although there are no studies, to our knowledge, examining the direct impact of laminin-α2 in the proliferation process in the context of LAMA2-CMD, the defects observed in this study suggest that a disruption in the interactions between laminin-211 and molecules/receptors in the extracellular environment may affect proliferation. Since laminin-211 is the main ligand of integrin-α7β1 during this particular fetal developmental stage and tissue, the lack of laminin-211 can be implicated in the perturbation of satellite cell activation, myoblast adhesion, and survival, which are processes known to be dependent on a functional laminin-211/integrin-α7β1 binding [30]. Multiple studies in both mouse models and LAMA2-CMD patients have confirmed that laminin-211 deficiency results in a decrease of the integrin-α7β1 receptor [30], [59], [61]. Research using C2C12 myoblasts revealed that overexpressing of integrin-α7β1 regulation improves the proliferation, adhesion, and migration of these cells [65]. These data suggest that integrin plays an important role in the cell proliferation process [65], and that the decrease of this receptor in LAMA2-CMD may explain why the proliferation process observed in this study is affected. However, further investigation is needed to fully understand the relationship between laminins and integrins in the context of cell proliferation.

We also investigated whether changing the culture conditions where the cells were growing from growth medium to differentiation medium had an impact on cell proliferation. At day 12,

the results of the assay of cells growing in differentiation media (**Figure 3.12 A**) followed the same pattern as the previous results for growth medium, when observing our results from *MKi67* gene expression (**Figure 3.11 A''**) and pH3-positive cell counting (**Figure 3.11 C**). In all cases, the absence of laminin-α2 impacted cell proliferation. Surprisingly, the data obtained from cells growing in the two different culture media revealed higher proliferation of cells growing in differentiation medium in WT rECM, particularly for the C2C12-KO cells (**Figure 3.12 A**). The proliferation was determined using the resazurin assay, which measures the reduction of resazurin (blue dye) to resorufin (pink dye) by the mitochondrial respiratory chain of living cells [66]. Thus, the amount of resorufin produced is directly proportional to the number of living cells. However, since this reaction only occurs in metabolically active cells [66], the increase in resorufin observed in the differentiation medium may indicate an increase in the metabolic rate of the cells rather than an increase in cell number. This hypothesis is supported by the observation that differentiated myoblasts display higher metabolic rates than proliferative myoblasts [67], [68]. In fact, during myogenic differentiation, an increase in mitochondrial activity is required [67]. Furthermore, the lower number of pH3-positive in the population of growing in differentiation medium when compared to growth medium in WT matrices demonstrates that the increased resorufin levels in the differentiation medium experimental situation do not correlate with higher proliferation (**Figure 3.12 B**). Overall, this data supports our previous findings, indicating that laminin-α2 has an impact in cell proliferation and that this effect persists regardless of whether or not the cells are induced to differentiate.

4.3 Absence of laminin-α2 affects differentiation and myotube formation

SM myogenesis is an organized and highly regulated process [69]. During this process, proliferating myoblasts start to express myogenin, exit the cell cycle, and differentiate into postmitotic cells. Subsequently, these cells begin to express proteins such as myosin heavy chain, and myoblast fusion occurs, resulting in the formation of multinucleated myotubes [69].

As laminin-211 is produced by both myoblasts and myotubes [70], we wanted to evaluate whether the absence of laminin-α2 could cause defects in myogenesis. To explore this, the expression level of *MyoG*, an early marker of myoblast differentiation, was analyzed in both *in*

vivo and *in vitro* models. Regrettably, it was not possible to analyze *MyoG* in the recellularized $dy^{W-/-}$ matrices of the 3D *in vitro* model due the difficulty of obtaining high numbers of $dy^{W-/-}$ fetuses. In the 2D *in vitro* model, the results reveal that C2C12-KO cells displayed lower levels of *MyoG* expression than C2C12-WT cells (**Figure 3.13 A'**). However, in WT rECM, C2C12-KO cells exhibit higher levels of *MyoG* expression when compared to C2C12-WT cells (**Figure 3.13 A''**). The expression levels of *MyoG* by cells of the *in vivo* model also showed a trend towards higher expression levels of *MyoG* in $dy^{W-/-}$ muscle than in WT (**Figure 3.13 A**). These findings suggest that the absence of laminin-211 may induce or deregulate the differentiation process. However, the higher levels of *MyoG* expressed in $dy^{W-/-}$ muscles, compared to WT muscles, seem to contradict the findings observed by Nunes *et al*. where $dy^{W-/-}$ muscles at E18.5 contained fewer myogenin-positive cells than WT individuals. Despite the fact that our results did not show statistical significant in *in vivo* muscles, it is important to note that different techniques were used: Nunes *et al.* quantified the number of myogenin protein, we quantified the expression level of the gene that encondes for myogenin, therefore mRNA levels. It is important to note that gene expression does not always correlate with protein abundance. Interestingly, the lower number of myogenin-positive cells observed by Nunes *et al*. may be related to the fact that $dy^{W-/-}$ individuals have a smaller cross-sectional area of muscles when compared to the ones of WT individuals. These observations are consistent with the results obtained using the 3D *in vitro* model, as we will discuss futher.

Even though we were not successful in labeling myogenin by immunohistochemistry, phalloidin labeling for actin filaments revealed that C2C12-KO cells tend to align more in matrices than C2C12-WT cells (**Figure 3.13 C'', E''**). This was observed on day 8 of culture, a period when higher levels of *MyoG* expression were detected in C2C12-KO cells cultured in matrices (**Figure 3.13 A''**).

Before myoblasts can fuse, they must align. The alignment of myoblasts is characterized by the organization of actin filaments and low expression of myosins [71]. It is only after alignment that myosins become expressed, enabling fusion and myotube formation [69], [71]. Therefore, the fact that C2C12-KO cells begin to align and express higher amounts of *MyoG* than C2C12-WT cells may suggest that the absence of laminin-211 could precociously initiate the myogenic differentiation program.

Inspired by this observation, we then cultivated the rECM in differentiation medium, followed by myosin staining. However, we noticed that only C2C12-WT cells were able to form multinucleated myotubes (**Figure 3.14 A - A''**) while C2C12-KO cells displayed the aligned pattern previously described, without any myosin labeling of the cells (**Figure 3.14 B - B'', D - D''**). Despite an extended period of culture up to 15 days, C2C12-KO cells never expressed myosin. These results suggest that, although C2C12-KO cells appear to initiate differentiation, they fail to express myosin, fuse and form multinucleated myotubes. Previous studies have reported the formation of unstable and abnormal myotubes accompanied by cell death in mice and humans In laminin-α2-deficient myoblasts [72]. Therefore, these findings support the critical role of laminin-211 in myoblast fusion, and justify the muscle fiber degeneration observed in humans and mice with LAMA2-CMD [22], [61], [73].

C2C12-WT cells in WT matrices not only form elongated and well-defined multinucleated myotubes but also exhibit the formation of multinucleated spherical structures (blue arrows and line dashed **Figure 3.14 A', A'''**), which are the only type of structures observed in $dy^{W-/-}$ dECM. Although this myotube conformation is normal in 3D cultures [74]–[76], Günay *et al.* consider it to be aberrant [77]. Rounded myotubes are also observed in human laminin-α2-deficient myoblasts [72], [77]. The fact that in $dy^{W-/-}$ matrices C2C12-WT cells do not form well-defined multinucleated myotubes suggests that the absence of laminin-211 in the extracellular medium negatively impacts the differentiation process. These observations strongly support that the composition of the ECM significantly affects cell behavior, and that the interactions between cells and ECM are crucial for proper myogenesis [78].

The observation that C2C12-KO cells elongate and align in both WT and $dy^{W-/-}$ matrices suggests that the absence of laminin-211 in the cellular component is a critical factor that cannot be compensated for by the presence of functional laminin-211 in the extracellular niche. Conversely, the lack of laminin-211 in the extracellular environment also affects cell behavior, as C2C12-WT cells cultured in a matrix without laminin-α2 are unable to form elongated and well-defined myotubes as well. Therefore, these findings suggest that the presence of functional laminin-211 in both the cellular and extracellular comparments is necessary for successful myogenesis to occur.

By using our 3D *in vitro* model, we have discovered that the absence of laminin-α2 in cells has a significant impact in the proliferation process. The inability of C2C12-KO cells to proliferate

may prompt them to enter a post-mitotic state, thus initiating the differentiation process. Consequently, these cells begin to express myogenin and align in matrices. Nonetheless, due to the absence of laminin-α2, they are unable to fuse and form multinucleated myotubes. We hypothesize that the failure of C2C12-KO cells cultured in matrices to form multinucleated myotubes could elucidate why Nunes *et al.* reported fewer myogenin-positive cells and smaller fibers in $dy^{W-/-}$ individuals .

The defects in differentiation and proliferation process resulting from the absence of laminin-α2 can potentially provide insight into the dysregulated pathways and mechanisms underlying LAMA2-CMD, which could be used as targets for novel therapeutic development.

4.4 Conclusion

Through this study, it was possible to improve the development of a 3D model for investigating interactions between the extracellular matrix and the cellular niches. The results indicate that the absence of laminin-α2 in these two components can have adverse effects on other proteins present in the extracellular matrix and could initiate fibrosis processes at an early stage. Additionally, the lack of laminin-α2 leads to defects in cell proliferation and differentiation. Although cells lacking laminin-α2 initiate differentiation earlier, they are unable to fuse and form myotubes. Even if either the cellular or extracellular compartments contains functional laminin-α2, the effects of its absence cannot be reversed.

Overall, LAMA2-CMD is a complex disease that affects multiple cellular mechanisms. A better understanding of the pathways perturbed by the absence of laminin- α2 is of great need for the search of effective therapies for this disease. The development of this 3D *in vitro* model is an important improvement that not only provides a valuable tool for studying the normal development of fetal skeletal muscle, but also has the potential to be a game changer in understanding the mechanisms involved in the early onset of muscular dystrophies and developing new therapies.

5 REFERENCES

[1] W. R. Frontera and J. Ochala, "Skeletal Muscle: A Brief Review of Structure and Function," *Behavior Genetics*, vol. 45, no. 2. Springer New York LLC, pp. 183–195, Mar. 04, 2015. doi: 10.1007/s00223-014-9915-y.

[2] K. Ahmad, S. Shaikh, S. S. Ahmad, E. J. Lee, and I. Choi, "Cross-Talk Between Extracellular Matrix and Skeletal Muscle: Implications for Myopathies," *Frontiers in Pharmacology*, vol. 11. Frontiers Media S.A., Feb. 28, 2020. doi: 10.3389/fphar.2020.00142.

[3] W. Zhang, Y. Liu, and H. Zhang, "Extracellular matrix: an important regulator of cell functions and skeletal muscle development," *Cell and Bioscience*, vol. 11, no. 1. BioMed Central Ltd, Dec. 01, 2021. doi: 10.1186/s13578-021-00579-4.

[4] K. C. Clause and T. H. Barker, "Extracellular matrix signaling in morphogenesis and repair," *Current Opinion in Biotechnology*, vol. 24, no. 5. pp. 830–833, Oct. 2013. doi: 10.1016/j.copbio.2013.04.011.

[5] S. Pompili, G. Latella, E. Gaudio, R. Sferra, and A. Vetuschi, "The Charming World of the Extracellular Matrix: A Dynamic and Protective Network of the Intestinal Wall," *Frontiers in Medicine*, vol. 8. Frontiers Media S.A., Apr. 16, 2021. doi: 10.3389/fmed.2021.610189.

[6] A. D. Theocharis, S. S. Skandalis, C. Gialeli, and N. K. Karamanos, "Extracellular matrix structure," *Advanced Drug Delivery Reviews*, vol. 97. Elsevier B.V., pp. 4–27, Feb. 01, 2016. doi: 10.1016/j.addr.2015.11.001.

[7] M. D. Grounds, "COMPLEXITY OF EXTRACELLULAR MATRIX AND SKELETAL MUSCLE REGENERATION," in *Skeletal Muscle Repair and Regeneration*, S. Schiaffino and T. Partridge, Eds., 2008, pp. 269–302. doi: DOI:10.1007/978-1-4020-6768-6_13.

[8] N. K. Karamanos *et al.*, "A guide to the composition and functions of the extracellular matrix," *FEBS Journal*, vol. 288, no. 24, pp. 6850–6912, Dec. 2021, doi: 10.1111/febs.15776.

[9] A. Ariza de Schellenberger, J. Bergs, I. Sack, and M. Taupitz, "The extracellular matrix as a target for biophysical and molecular magnetic resonance imaging," in *Quantification of Biophysical Parameters in Medical Imaging*, Springer International Publishing, 2018, pp. 123–150. doi: 10.1007/978-3-319-65924-4_6.

[10] V. S. LeBleu, B. MacDonald, and R. Kalluri, "Structure and function of basement membranes," *Experimental Biology and Medicine*, vol. 232, no. 9. pp. 1121–1129, Oct. 2007. doi: 10.3181/0703-MR-72.

[11] R. Jayadev and D. R. Sherwood, "Basement membranes," *Current Biology*, vol. 27, no. 6. Cell Press, pp. R207–R211, Mar. 20, 2017. doi: 10.1016/j.cub.2017.02.006.

[12] A. G. Borycki, "The myotomal basement membrane: Insight into laminin-111 function and its control by Sonic hedgehog signaling," *Cell Adhesion and Migration*, vol. 7, no. 1. Taylor and Francis Inc., pp. 72–81, 2013. doi: 10.4161/cam.23411.

[13] P. Rifes *et al.*, "Redefining the role of ectoderm in somitogenesis: A player in the formation of the fibronectin matrix of presomitic mesoderm," *Development*, vol. 134, no. 17, pp. 3155–3165, Sep. 2007, doi: 10.1242/dev.003665.

[14] S. Thorsteinsdottir, M. Deries, A. S. Cachaço, and F. Bajanca, "The extracellular matrix dimension of skeletal muscle development," *Developmental Biology*, vol. 354, no. 2. Academic Press Inc., pp. 191–207, 2011. doi: 10.1016/j.ydbio.2011.03.015.

[15] G. Hollway and P. Currie, "Vertebrate myotome development," *Birth Defects Research Part C - Embryo Today: Reviews*, vol. 75, no. 3. pp. 172–179, Sep. 2005. doi: 10.1002/bdrc.20046.

[16] M. Deries, R. Schweitzer, and M. J. Duxson, "Developmental fate of the mammalian myotome," *Developmental Dynamics*, vol. 239, no. 11, pp. 2898–2910, Nov. 2010, doi: 10.1002/dvdy.22425.

[17] J. Gros, M. Manceau, V. Thomé, and C. Marcelle, "A common somitic origin for embryonic muscle progenitors and satellite cells," *Nature*, vol. 435, no. 7044, pp. 954–958, Jun. 2005, doi: 10.1038/nature03572.

[18] H. A. Asfour, M. Z. Allouh, and R. S. Said, "Myogenic regulatory factors: The orchestrators of myogenesis after 30 years of discovery," *Exp Biol Med*, vol. 243, no. 2, pp. 118–128, Jan. 2018, doi: 10.1177/1535370217749494.

[19] M. Deries, A. B. Gonçalves, and S. Thorsteinsdóttir, "Skeletal muscle development-from stem cells to body movement," in *Concepts and Applications of Stem Cell Biology*, 2020, pp. 159–169.

[20] M. Deries, A. B. Gonçalves, R. Vaz, G. G. Martins, G. Rodrigues, and S. Thorsteinsdóttir, "Extracellular matrix remodeling accompanies axial muscle development and morphogenesis in the mouse," *Developmental Dynamics*, vol. 241, no. 2, pp. 350–364, Feb. 2012, doi: 10.1002/dvdy.23703.

[21] F. Bajanca *et al.*, "Integrin α6β1-laminin interactions regulate early myotome formation in the mouse embryo," *Development*, vol. 133, no. 9, pp. 1635–1644, May 2006, doi: 10.1242/dev.02336.

[22] A. M. Nunes *et al.*, "Impaired fetal muscle development and JAK-STAT activation mark disease onset and progression in a mouse model for merosin-deficient congenital muscular dystrophy," *Hum Mol Genet*, vol. 26, no. 11, pp. 2018–2033, Jun. 2017, doi: 10.1093/hmg/ddx083.

[23] P. Bailey, T. Holowacz, and A. B Lassar, "The origin of skeletal muscle stem cells in the embryo and the adult," *Curr Opin Cell Biol*, vol. 13, pp. 679–689, 2001.

[24] P. Mohassel, A. Reghan Foley, and C. G. Bönnemann, "Extracellular matrix-driven congenital muscular dystrophies," *Matrix Biology*, vol. 71–72. Elsevier B.V., pp. 188–204, Oct. 01, 2018. doi: 10.1016/j.matbio.2018.06.005.

[25] R. M. Lovering, N. C. Porter, and R. J. Bloch, "The Muscular Dystrophies: From Genes to Therapies," *Phys Ther*, pp. 1372–1388, 2005, [Online]. Available: http://www.mdausa.org/

[26] P. M. Van Ry, T. M. Fontelonga, P. Barraza-Flores, A. Sarathy, A. M. Nunes, and D. J. Burkin, "ECM-related myopathies and muscular dystrophies: Pros and cons of protein therapies," *Compr Physiol*, vol. 7, no. 4, pp. 1519–1536, Oct. 2017, doi: 10.1002/cphy.c150033.

[27] P. D. Yurchenco, K. K. McKee, J. R. Reinhard, and M. A. Rüegg, "Laminin-deficient muscular dystrophy: Molecular pathogenesis and structural repair strategies," *Matrix Biology*, vol. 71–72. Elsevier B.V., pp. 174–187, Oct. 01, 2018. doi: 10.1016/j.matbio.2017.11.009.

[28] M. Kanagawa and T. Toda, "The genetic and molecular basis of muscular dystrophy: Roles of cell-matrix linkage in the pathogenesis," *Journal of Human Genetics*, vol. 51, no. 11. pp. 915–926, Nov. 2006. doi: 10.1007/s10038-006-0056-7.

[29] K. I. Gawlik and M. Durbeej, "Skeletal muscle laminin and MDC1A: pathogenesis and treatment strategies," 2011. [Online]. Available: http://www.skeletalmusclejournal.com/content/1/1/9

[30] P. Barraza-Flores, C. R. Bates, A. Oliveira-Santos, and D. J. Burkin, "Laminin and Integrin in LAMA2-Related Congenital Muscular Dystrophy: From Disease to Therapeutics,"

Frontiers in Molecular Neuroscience, vol. 13. Frontiers Media S.A., Feb. 11, 2020. doi: 10.3389/fnmol.2020.00001.

[31] D. U. Kemaladewi *et al.*, "A mutation-independent approach for muscular dystrophy via upregulation of a modifier gene," *Nature*, vol. 572, no. 7767, pp. 125–130, Aug. 2019, doi: 10.1038/s41586-019-1430-x.

[32] A. Sarkozy, A. R. Foley, A. A. Zambon, C. G. Bönnemann, and F. Muntoni, "LAMA2-Related Dystrophies: Clinical Phenotypes, Disease Biomarkers, and Clinical Trial Readiness," *Frontiers in Molecular Neuroscience*, vol. 13. Frontiers Media S.A., Aug. 05, 2020. doi: 10.3389/fnmol.2020.00123.

[33] F. Gattazzo, A. Urciuolo, and P. Bonaldo, "Extracellular matrix: A dynamic microenvironment for stem cell niche," *Biochimica et Biophysica Acta - General Subjects*, vol. 1840, no. 8. Elsevier, pp. 2506–2519, 2014. doi: 10.1016/j.bbagen.2014.01.010.

[34] K. J. Wilschut, V. B. Ling, and H. S. Bernstein, "Concise Review: Stem Cell Therapy for Muscular Dystrophies," *Stem Cells Transl Med*, vol. 1, no. 11, pp. 833–842, Nov. 2012, doi: 10.5966/sctm.2012-0071.

[35] N. A. Dumont, Y. X. Wang, and M. A. Rudnicki, "Intrinsic and extrinsic mechanisms regulating satellite cell function," *Development (Cambridge)*, vol. 142, no. 9. Company of Biologists Ltd, pp. 1572–1581, 2015. doi: 10.1242/dev.114223.

[36] E. Fuchs, T. Tumbar, and G. Guasch, "Review Socializing with the Neighbors: Stem Cells and Their Niche fied by experiments in which the fate of ESCs is moni-tored following their subcutaneous injection into nude mice. ESCs isolated from a blastocyst-stage mouse em," 2004.

[37] M.-G. Barbu *et al.*, "Skeletal Muscle Stem Cell Niche from Birth to Old Age," in *Background and Management of Muscular Atrophy*, J. Cseri, Ed., 2020. [Online]. Available: www.intechopen.com

[38] D. Rana, H. Zreiqat, N. Benkirane-Jessel, S. Ramakrishna, and M. Ramalingam, "Development of decellularized scaffolds for stem cell-driven tissue engineering," *Journal of Tissue Engineering and Regenerative Medicine*, vol. 11, no. 4. John Wiley and Sons Ltd, pp. 942–965, Apr. 01, 2017. doi: 10.1002/term.2061.

[39] D. Yaffe and O. Saxel, "Serial passaging and differentiation of myogenic cells isolated from dystrophic mouse muscle," *Nature*, vol. 270, pp. 725–727, 1977, doi: https://doi.org/10.1038/270725a0.

[40] E. Falcieri *et al.*, "C2C12 murine myoblasts as a model of skeletal muscle development: morpho-functional characterization," 2004.

[41] Melo, C. E. M. de and Carlos, A. R. C. M. "The impact of Lama2-deficiency on cell cycle regulation and survival. *Repositório da Universidade de Lisboa,* 2022, https://repositorio.ul.pt/handle/10451/53636 (2022).

[42] M. Kapałczyńska *et al.*, "2D and 3D cell cultures – a comparison of different types of cancer cell cultures," *Archives of Medical Science*, vol. 14, no. 4, pp. 910–919, 2018, doi: 10.5114/aoms.2016.63743.

[43] P. M. Crapo, T. W. Gilbert, and S. F. Badylak, "An overview of tissue and whole organ decellularization processes," *Biomaterials*, vol. 32, no. 12. pp. 3233–3243, Apr. 2011. doi: 10.1016/j.biomaterials.2011.01.057.

[44] Y. H. Tan, H. R. Helms, and K. H. Nakayama, "Decellularization Strategies for Regenerating Cardiac and Skeletal Muscle Tissues," *Frontiers in Bioengineering and Biotechnology*, vol. 10. Frontiers Media S.A., Feb. 28, 2022. doi: 10.3389/fbioe.2022.831300.

[45] P. Gameiro dos Santos, A. R. Soares, S. Thorsteinsdóttir, and G. Rodrigues, "Preparation of 3D Decellularized Matrices from Fetal Mouse Skeletal Muscle for Cell Culture," *Journal of Visualized Experiments*, no. 193, Mar. 2023, doi: 10.3791/65069.

[46] M. W. McCrary, D. Bousalis, S. Mobini, Y. H. Song, and C. E. Schmidt, "Decellularized tissues as platforms for in vitro modeling of healthy and diseased tissues," *Acta Biomaterialia*, vol. 111. Acta Materialia Inc, pp. 1–19, Jul. 15, 2020. doi: 10.1016/j.actbio.2020.05.031.

[47] W. Kuang, H. Xu, P. H. Vachon, and E. Engvall, "Disruption of the lama2 Gene in Embryonic Stem Cells: Laminin a2 Is Necessary for Sustenance of Mature Muscle Cells," 1998.

[48] B. Ringelmann *et al.*, "Expression of Laminin 1, 2, 4, and 5 Chains, Fibronectin, and Tenascin-C in Skeletal Muscle of Dystrophic 129ReJ dy/dy Mice," 1999. [Online]. Available: http://www.idealibrary.com

[49] A. C. Silva *et al.*, "Three-dimensional scaffolds of fetal decellularized hearts exhibit enhanced potential to support cardiac cells in comparison to the adult," *Biomaterials*, vol. 104, pp. 52–64, Oct. 2016, doi: 10.1016/j.biomaterials.2016.06.062.

[50] B. M. De Oliveira *et al.*, "Quantitative proteomic analysis reveals metabolic alterations, calcium dysregulation, and increased expression of extracellular matrix proteins in Laminin α2 Chain-deficient muscle," *Molecular and Cellular Proteomics*, vol. 13, no. 11, pp. 3001–3013, Nov. 2014, doi: 10.1074/mcp.M113.032276.

[51] H. Kölbel, D. Hathazi, M. Jennings, R. Horvath, A. Roos, and U. Schara, "Identification of candidate protein markers in skeletal muscle of laminin-211-deficient CMD type 1A-patients," *Front Neurol*, vol. 10, no. MAY, 2019, doi: 10.3389/fneur.2019.00470.

[52] E. Van Lunteren, M. Moyer, and P. Leahy, "Gene expression profiling of diaphragm muscle in 2-laminin (merosin)-deficient dy/dy dystrophic mice," *Physiol Genomics*, vol. 25, pp. 85–95, 2006, doi: 10.1152/physiolgenomics.00226.2005.-Deficiency.

[53] C. Alexakis, T. Partridge, and G. Bou-Gharios, "Implication of the satellite cell in dystrophic muscle fibrosis: a self-perpetuating mechanism of collagen overproduction," *Am J Physiol Cell Physiol*, vol. 293, pp. 661–669, 2007, doi: 10.1152/ajpcell.00061.2007.-Because.

[54] C. J. Mann *et al.*, "Aberrant repair and fibrosis development in skeletal muscle," *Skeletal Muscle*, vol. 1, no. 1. May 04, 2011. doi: 10.1186/2044-5040-1-21.

[55] T. Mehuron, A. Kumar, L. Duarte, J. Yamauchi, A. Accorsi, and M. Girgenrath, "Dysregulation of matricellular proteins is an early signature of pathology in laminin-deficient muscular dystrophy," *Skelet Muscle*, vol. 4, no. 1, Jul. 2014, doi: 10.1186/2044-5040-4-14.

[56] A. Accorsi, M. L. Cramer, and M. Girgenrath, "Fibrogenesis in LAMA2-Related Muscular Dystrophy Is a Central Tenet of Disease Etiology," *Frontiers in Molecular Neuroscience*, vol. 13. Frontiers Media S.A., Feb. 04, 2020. doi: 10.3389/fnmol.2020.00003.

[57] A. Accorsi, T. Mehuron, A. Kumar, Y. Rhee, and M. Girgenrath, "Integrin dysregulation as a possible driver of matrix remodeling in Laminin-deficient congenital muscular dystrophy (MDC1A)," *J Neuromuscul Dis*, vol. 2, no. 1, pp. 51–61, 2015, doi: 10.3233/JND-140042.

[58] K. I. Gawlik and M. Durbeej, "A Family of Laminin α2 Chain-Deficient Mouse Mutants: Advancing the Research on LAMA2-CMD," *Frontiers in Molecular Neuroscience*, vol. 13. Frontiers Media S.A., Apr. 21, 2020. doi: 10.3389/fnmol.2020.00059.

[59] B L Hodges, Y K Hayashi, I Nonaka, W Wang, K Arahata, and S J Kaufman, "Altered expression of the alpha7beta1 integrin in human and murine muscular dystrophies," *Journal of Cell Science 110, 2873-2881*, 1997, doi: doi:10.1242/jcs.110.22.2873.

[60] P. H. Vachon *et al.*, "Integrins (α7β1) in muscle function and survival disrupted expression in merosin-deficient congenital muscular dystrophy," *Journal of Clinical Investigation*, vol. 100, no. 7, pp. 1870–1881, Oct. 1997, doi: 10.1172/JCI119716.

[61] P. H. Vachon, F. Loechel, H. Xu, U. M. Wewer, and E. Engvall, "Merosin and Laminin in Myogenesis; Specific Requirement for Merosin in Myotube Stability and Survival," *The Jornal of Cell Biology* , vol. 134, pp. 1483–1497, 1996.

[62] M. Girgenrath, C. A. Kostek, and J. B. Miller, "Diseased muscles that lack dystrophin or laminin-α2 have altered compositions and proliferation of mononuclear cell populations," *BMC Neurol*, vol. 5, Apr. 2005, doi: 10.1186/1471-2377-5-7.

[63] S. L. Goodman and S. D. Hauschka, "Laminin Alters Cell Shape and Stimulates Motility and Proliferation of Murine Skeletal Myoblasts," 1988.

[64] M. A. Mat Afandi, M. Maarof, S. R. Chowdhury, and R. Bt. Hj. Idrus, "Synergistic Effect of Laminin and Epidermal Growth Factor on Biological and Morphological Properties of Co-Cultured Myoblasts and Fibroblasts," *Tissue Eng Regen Med*, vol. 17, no. 6, pp. 835–845, Dec. 2020, doi: 10.1007/s13770-020-00283-3.

[65] J. Liu, D. J. Burkin, and S. J. Kaufman, "Increasing 7 1-integrin promotes muscle cell proliferation, adhesion, and resistance to apoptosis without changing gene expression," *Am J Physiol Cell Physiol*, vol. 294, pp. 627–640, 2008, doi: 10.1152/ajpcell.00329.2007.-The.

[66] · Zhang, "Assay of mitochondrial functions by resazurin in vitro," 2004. [Online]. Available: http://www.ChinaPhar.com

[67] J. Sin *et al.*, "Mitophagy is required for mitochondrial biogenesis and myogenic differentiation of C2C12 myoblasts," *Autophagy*, vol. 12, no. 2, pp. 369–380, Jan. 2016, doi: 10.1080/15548627.2015.1115172.

[68] M. Jang, J. Scheffold, L. M. Røst, H. Cheon, and P. Bruheim, "Serum-free cultures of C2C12 cells show different muscle phenotypes which can be estimated by metabolic profiling," *Sci Rep*, vol. 12, no. 1, Dec. 2022, doi: 10.1038/s41598-022-04804-z.

[69] V. Andr6s and K. Walsh, "Myogenin Expression, Cell Cycle Withdrawal, and Phenotypic Differentiation Are Temporally Separable Events that Precede Cell Fusion upon Myogenesis," 1996.

[70] F. Schuler and L. M. Sorokin, "Expression of laminin isoforms in mouse myogenic cells in vitro and in vivo," *Journal of Cell Science 108, 3795-3805* , 1995.

[71] N. T. Swailes, P. J. Knight, and M. Peckham, "Actin filament organization in aligned prefusion myoblasts," 2004.

[72] V. K. Vishnudas and J. B. Miller, "Ku70 regulates Bax-mediated pathogenesis in laminin-α2-deficient human muscle cells and mouse models of congenital muscular dystrophy," *Hum Mol Genet*, vol. 18, no. 23, pp. 4467–4477, 2009, doi: 10.1093/hmg/ddp399.

[73] Y. K. Hayashi *et al.*, "Massive muscle cell degeneration in the early stage of merosin-deficient congenital muscular dystrophy," 2000. [Online]. Available: www.elsevier.com/locate/nmd

[74] A. Bettadapur *et al.*, "Prolonged Culture of Aligned Skeletal Myotubes on Micromolded Gelatin Hydrogels," *Sci Rep*, vol. 6, Jun. 2016, doi: 10.1038/srep28855.

[75] G. Cerino *et al.*, "Three dimensional multi-cellular muscle-like tissue engineering in perfusion-based bioreactors," *Biotechnol Bioeng*, vol. 113, no. 1, pp. 226–236, Jan. 2016, doi: 10.1002/bit.25688.

[76] J. A. DeQuach *et al.*, "Simple and high yielding method for preparing tissue specific extracellular matrix coatings for cell culture," *PLoS One*, vol. 5, no. 9, 2010, doi: 10.1371/journal.pone.0013039.

[77] K. A. Günay *et al.*, "Myoblast mechanotransduction and myotube morphology is dependent on BAG3 regulation of YAP and TAZ," *Biomaterials*, vol. 277, Oct. 2021, doi: 10.1016/j.biomaterials.2021.121097.

[78] N. Osses and E. Brandan, "ECM is required for skeletal muscle differentiation independently of muscle regulatory factor expression," *Am J Physiol Cell Physiol*, vol. 282, pp. 383–394, 2002, doi: 10.1152/ajpcell.00322.2001.-Transcription.

6

ANNEXES

Table A1. List of primers used in genotyping.

	Primers	Sequence
dy$^{W-/-}$ mice	Primer 1	5' ACTGCCCTTTC TCACCCACCCTT 3'
	Primer 2	5' GTTGATGCGCTTGGGACTG 3'
	Primer 3	5' GTCGACGACGACAGTACTGGCCTCAG 3'

Table A.2. PCR protocol for mice genotyping.

Step	Temperature (℃)	Time	Notes
1	94	2 min	
2		20 sec	
3	65	15 sec	
4	68	10 sec	
5	-	-	Repeat steps 2-4 for 10 cycles
6	94	15 sec	
7	60		
8	72	10	
9	-	-	Repeat steps 6-8 for 28 cycles
10	72	2 min	
11	12		Hold

Table A.3. List of primers used for gene expression analysis.

Gene	Primer	Sequence
Arbp0	Forward	5′ CTTTGGGCATCACCACGAA 3′
	Reverse	5′ GCTGGCTCCCACCTTGTCT 3′
Lama2	Forward	5′ TGAAAGCAAGGCCAGAAGTCA 3′
	Reverse	5′ ACAAAACCAGGCTTGGGGAA 3′
Mki67	Forward	5′ ATCCTGTCACTCCAGATCAGAACTC 3′
	Reverse	5′ ATCCCGACATTCTCTGCAGATGC 3′
MyoG	Forward	5′ GTCCCAACCCAGGAGATCAT 3′
	Reverse	5′ CCACGATGGACGTAAGGGAG 3′
Lama5	Forward	5′ GCACCCTGGTGCTCTTCTAT 3′
	Reverse	5′ GAAACACTTGGATCGCCTTGC 3′
Col4a1	Forward	5′ GACTTTGCCCCAACAGGAGA 3′
	Reverse	5′ CTTTCCCAGGTTTTCCCCGA 3′
Col1a1	Forward	5′ CGATGGATTCCCGTTCGAGT 3′
	Reverse	5′ CGATCTCGTTGGATCCCTGG 3′
Fibronectin	Forward	5′ CCACCATTACTGGTCTGGAG 3′
	Reverse	5′ TGGAAGGGTAACCAGTTGGG 3′
Hspg2	Forward	5′ ACTCATCATCAGACGCACGG 3′
	Reverse	5′ AGGAAGTCTCGATGCGGATG 3′

Table A.4- Real Time-qPCR protocol

Real Time PCR system	Setting/ Mode	Polymerase Activation and DNA Denaturation	Denaturation at 95°C	Annealing /Extension and Plate Read at 60°C	Cycles	Melting Curve Analysis

Bio-Rad CFX96™	SYBR only	30 sec at 95°C	5 sec	15 sec	40	65-95°C, 0.5°C increments at 5 sec/step

Table A.5. Antibodies used for western blot and immunohistochemistry, and respective dilutions.

						Western Blot	Immuno-histo-chemistry
Antibody	**Clonality**	**Raised in**	**Primary/ Secondary**	**Brand**	**Catalog Number**	**Dilution**	
α-Fibronectin	Polyclonal	Rabbit	Primary	Sigma	F-3648	1: 2000	1: 250
α-Laminin α2	Monoclonal	Rat		Sigma	L-0663	1:1000	1: 50
α-pan-Laminin	Polyclonal	Rabbit		Sigma	L- 9393	1:1000	1:200
α-Collagen I	Polyclonal	Rabbit		abcam	ab21285	1:1000	1:100
α-Collagen IV	Monoclonal	Rabbit		Millipore	Millipore	1:1000	1:250
α-phospho-histone-3	Polyclonal	Rabbit		Merk Millipore	06-570	-	1:200
α-Myosin Heavy Chain	Monoclonal	Mouse		D.S.H.B.	MF20	-	1:50
α-Mouse Alexa 488	Polyclonal	Goat	Secondary	Molecular Probes	A−11017	-	1:1000

α-Mouse Alexa 568	Polyclonal	Goat		Molecu-lar Probes	A−11019	-	1:1000
α-Rabbit Alexa 568	Polyclonal	Goat		Molecu-lar Probes	A−11070	-	1:1000
α-Rabbit Alexa 568	Polyclonal	Goat		Molecu-lar Probes	A21069	-	1:1000
Phalloidin Alexa 488	-	-	Dye	Thermo Fisher Sci.	A12379	-	1:250
Methyl Green	-	-	Dye			-	1:150
HRP-α-Mouse IgG	Polyclonal	Goat	Secondary	abcam	ab205719	1:5000	-
HRP-α-Rabbit IgG	Polyclonal	Goat		abcam	ab205718	1:5000	-
HRP-α- Rat IgG	Polyclonal	Goat		Abcam	ab205720	1:5000	-